

Rediscovery of a rare and endangered *Apostolepis* (Serpentes: Dipsadidae): reassessing species boundaries and phylogenetic relationships using integrative approaches

Omar M. Entiauspe-Neto^{1,2}, Alejandro R. Giraudo³, Thaís B. Guedes^{4,5}, Arthur Tiutenko⁶, Márcio Borges-Martins⁷ & Claudia Koch⁸

¹Laboratório de Coleções Zoológicas, Instituto Butantan, 05503-90, Av. Vital Brazil, 1500, Butantã, São Paulo, São Paulo, Brazil ²Programa de Pós-Graduação em Zoologia, Departamento de Zoologia, Instituto de Biociências, Universidade de São Paulo, Rua do Matão, 321, Travessa 14, 05508-090, São Paulo, São Paulo, Brazil

³ Laboratorio de Biodiversidad y Conservación, Instituto Nacional de Limnología (CONICET, UNL), FHUC (UNL), José Maciá 1933, Santo Tomé, 3016, Santa Fe, Argentina

⁴Departamento de Biodiversidade, Instituto de Biociências, Universidade Estadual Paulista "Júlio de Mesquita Filho", Rio Claro, 13506-900, São Paulo, Brazil

⁵ Gothenburg Global Biodiversity Center, University of Gothenburg, Department of Biological and Environmental Sciences, Box 461, SE-405 30, Göteborg, Sweden

⁶ Friedrich-Alexander-Universität Erlangen-Nürnberg, Schloßplatz 4, 91054, Erlangen, Germany

⁷ Programa de Pós-graduação em Biologia Animal, Departamento de Zoologia, Instituto de Biociências, Universidade Federal do Rio Grande do Sul, Av. Bento Gonçalves, 91501-970, Porto Alegre, Rio Grande do Sul, Brazil

⁸ Leibniz Institute for the Analysis of Biodiversity Change, Museum Koenig Bonn, Adenauerallee 160, 53113, Bonn, Germany

Corresponding author: OMAR M. Entiauspe-Neto, e-mail: entiauspe@gmail.com

Manuscript received: 1 September 2024 Accepted: 18 December 2024 by Edgar Lehr

Abstract. *Apostolepis* is a diverse genus of small and fossorial dipsadid snakes, comprising 34 species ranging from Colombia southwards into Argentina. Most species are known from small series and very little is known regarding their phylogenetic relationships, morphological variation and diagnoses, which has caused a widespread historical taxonomic instability for the genus. Its southernmost representative, *Apostolepis quirogai*, is known solely from three specimens from the Mesopotamian and Uruguayan Savannas, with no new records in the last two decades. Its rarity, puzzling external morphology, and unique coloration pattern have significantly contributed to an uncertain systematic relationship for this species. We report the rediscovery of *A. quirogai*, providing an integrative species delimitation based on multivariate analyses, external morphology and molecular systematics, a redescription, an updated account of its morphological variation, geographic distribution, and a description of its cranial osteology. We provide a new phylogenetic hypothesis for the Elapomorphini, where we consistently recover *A. quirogai* nested within the *Apostolepis assimilis* species group, which is redefined and discussed here. We also provide a comparative osteological analysis of skull morphology for *Apostolepis*, providing insights into diagnostic characters and cranial evolution for the group.

Key words. Elapomorphini, integrative taxonomy, morphology, Neotropics, osteology, Squamata.

Introduction

The tribe Elapomorphini Jan, 1862 is a diverse group of dipsadid groundsnakes, encompassing five genera that contain approximately 50 species of small- to medium-sized snakes, which have mostly nocturnal, fossorial or cryptozoic habits (Entiauspe-Neto et al. 2022, Ferrarezzi 1993, Harvey 1999). The Elapomorphini genera, *Apostolepis* Cope, 1862, *Coronelaps* Lema & Hofstadler-Deiques, 2010, *Elapomorphus* Wiegmann (in Fitzinger), 1843, *Parapostolepis* Amaral, 1930, and *Phalotris* Cope,

1862, remain diagnosed based on putatively synapomorphic coloration, head scalation, osteological, and hemipenial characters, and have not yet been evaluated under a phylogenetic framework (Ferrarezzi 1993, Lema 2001, Lema & Hofstadler-Deiques 2010, Zaher et al. 2018). *Apostolepis* is the most diverse genus of the tribe, with 34 species that are widely distributed at East of the Andes, and most of this diversity occurs within the South American Dry Diagonal and its open habitats (Entiauspe-Neto et al. 2022, Ferrarezzi 1993). *Apostolepis* species can be diagnosed from other Elapomorphini genera for having a pair

of prefrontals (possibly) fused to internasals, a black tail tip (except for *Apostolepis quinquelineata* Boulenger, 1896), 15 dorsal rows, and lacking a postorbital bone (Entiauspe-Neto et al. 2019, 2020a, 2021a,b, 2022, Ferrarezzi 1993).

As most Apostolepis species occur within the Caatinga, Cerrado, and Chaco ecoregions, very little is known regarding the diversity of this genus in the Mesopotamian and Uruguayan Savannas. The Mesopotamian and Uruguayan Savannas are characterized by extensive grassland and shrubland areas, with gallery forests and palm tree savannas, located in the southern half of Rio Grande do Sul state in Brazil, the entire territory of Uruguay, and part of the provinces of Corrientes and Misiones in Argentina (ALVARES et al., 2021, OLSON et al., 2001). Other classifications and delimitations have also been proposed for this area of grasslands, such as the Uruguayan District from the Pampean Province (CABRERA & WILLINK 1973), and the Campos Subregion from the Rio de La Plata Grasslands (SORIANO et al. 1992), with conflicting delimitations as to whether it is closely related to Chacoan ecoregion (CABRE-RA & WILLINK 1973, MORRONE 2014) or just a cohesive unit of tropical and subtropical grasslands (Olson et al. 2001). Hereafter, we consider Uruguayan and Mesopotamian Savannas to be synonymous with open grassland formations. Only two species have been recorded to this ecoregion: Apostolepis dimidiata (JAN, 1862) and Apostolepis quirogai GIRAUDO & SCROCCHI, 1998, which are known to occur in sympatry (GIRAUDO & SCROCCHI 1998). The first species, A. dimidiata, has its core distribution in the Cerrado, with southernmost records in the Uruguayan Savanna of Corrientes, Argentina, close to the border with Brazil (EN-TIAUSPE-NETO et al. 2019, 2022). The latter species, A. quirogai, is the southernmost representative of Apostolepis, and appears to be endemic to a small portion of Uruguayan Savanna, with two disjunct populations in Argentina and Brazil (GIRAUDO & SCROCCHI 1998, LEMA 2001).

Apostolepis quirogai was described based on two specimens (FML 06000, adult female holotype, and FML 06001, adult male paratype) from Posadas, Misiones, Argentina (GIRAUDO & SCROCCHI 1998). The authors provide a description of external morphology and an overview of the retracted and uneverted hemipenis from the male paratype. Shortly after, a third specimen (MCP 12185, adult male) was reported from Santo Ângelo, Rio Grande do Sul, Brazil, extending the distribution of the species 180 km southwest from its type locality (LEMA & CAPPEL-LARI 2001). LEMA et al. (2004) would later describe its external morphology, with a short description of its everted hemipenes and dry prepared skull. No other specimens have been formally reported since 2001. Considering its restricted distribution, continued decline of habitat quality, and lack of new records, A. quirogai has been considered a threatened species, evaluated as Endangered (EN) in Brazil (SALVE 2019). All specimens were collected by third parties or found dead, and therefore, nothing is currently known regarding its natural history.

The systematic relationships of *A. quirogai* are also unknown. Although there are no comprehensive phylogenet-

ic hypotheses for Apostolepis, most authors have followed the intrageneric species-group arrangement proposed by FERRAREZZI (1993), in an unpublished master dissertation. Based on external morphology, Lema (2001) and LEMA et al. (2004) assigned this species to the A. dimidiata species group. Later, FERRAREZZI et al. (2005) provided a phylogenetic hypothesis to the A. assimilis and A. dorbignyi groups, in which these authors argued that Apostolepis arenaria Rodrigues, 1993, Apostolepis gaboi Rodrigues, 1993, and A. quirogai were possibly members of the A. assimilis species group (FERRAREZZI et al. 2005: 217). These authors stated that they did not have enough data to include A. quirogai in their phylogenetic analysis, and as it lacked most of the diagnostic features of the external morphology of the A. assimilis group, it could be a sister species to this clade (FERRAREZZI et al. 2005: 224). Both A. arenaria and A. gaboi are striped, psammophilous taxa restricted to the sand dunes of the left and right margins of the São Francisco River, respectively, in Bahia, northeastern Brazil (Rod-RIGUES 1993). These authors also argue that, due to their similar morphology and geographic distribution, A. arenaria and A. gaboi likely are closely related species (FER-RAREZZI et al. 2005: 224).

The conflicting views regarding the taxonomy and systematics of A. quirogai are likely explained by its rarity and unique external morphology. For instance, its wide dorsolateral black bands and a uniformly black venter are unknown in any species of the A. assimilis group. However, its slightly projected rostral scale, rounded snout, a wide white nuchal collar, and a conspicuous white snout blotch do not occur in the A. dimidiata group. Furthermore, it differs from other species groups, such as A. flavotorquata, A. nigrolineata, A. longicaudata, and A. nigroterminata (sensu Ferrarezzi 1993), by lacking thin dorsal stripes, and by having a black terminal scale and posterior temporals, among other characters of external morphology (Fer-RAREZZI 1993). However, molecular data is unavailable for most species, as the most recent phylogenetic hypothesis for Elapomorphini covers only 11 out of 50 known species, and two genera (Coronelaps and Parapostolepis) remain unsampled (Entiauspe-Neto et al. 2022).

In light of these questions, we have reviewed scientific collections in the Americas, Asia, and Europe, looking for new specimens and tissue samples of A. quirogai. In this work, we report the rediscovery of A. quirogai based on five new individuals from different new localities, the first specimens known since its last record in 2001, providing a redescription, an updated account of its morphological variation and geographic distribution, inferring its molecular phylogenetic relationships among other Elapomorphini genera, and providing a description of its cranial osteology. Based on molecular systematics and morphology, we provide an overview and a new diagnosis for the A. assimilis species group, discussing its putative synapomorphies and allocating three additional species to the group. Furthermore, we provide a comparative osteological analysis of skull morphology for Apostolepis, discussing diagnostic characters and cranial evolution for the group.

Materials and methods Morphological analyses

We examined a total of 761 specimens of Apostolepis (Supplementary Material 1, acronyms according to SABAJ [2019]), of which 23 belong to two species that occur in the Uruguayan Savanna. Scale counts follow DowLing (1951) and Peters (1964). Sex determination was done with a ventral incision in the base of the tail or by probing. An emended diagnosis is based on the nomenclature used by Entiauspe-Neto et al. (2020a). We refrained from including literature records that did not include verifiable morphological information associated with the purported individuals (see Entiauspe-Neto et al. (2021b) for discussion on sources of doubtful records for Elapomorphini). We measured head length and head width to the nearest 0.01 mm using a dial caliper; and snout-vent length and tail length to the nearest 1 mm using a flexible ruler. We measured scales on the right side of the head and defined our measurement within the description when appropriate. We calculate the Extent of Occurrence and Area of Occupancy (based on 2 km cell width) by using the Geospatial Conservation Assessment Tool (GeoCAT, BACHMANN et al. 2011), applied over the verified geographical coordinates of verified records.

In order to confirm the identification of new specimens, tentatively assigned to *A*. cf. *quirogai* [females = 3, males = 2] specimens, we generated a dataset (Dataset 1, Supplementary File 1, Supplementary Material 1) of quantitative and qualitative diagnostic morphological characters to be evaluated in a series of Operational Taxonomic Units (OTUs) of the *A. assimilis* and *A. dimidiata* species groups (*A. arenaria* [female = 1]; *Apostolepis assimilis* (ReINHARDT, 1861) [females = 12, males = 11]; *Apostolepis cearensis* Gomes, 1915 [females = 8, males = 7]; *A. dimidiata* [females = 5, males = 4]; *A. gaboi* [females = 11, males = 12]; *Apostolepis sanctaeritae* Werner, 1924 [females = 10, males = 7]; *A. quirogai* [females = 1, males = 2]), which underwent sex determination and are considered to be putatively adults (N = 96).

We analyzed: (1) snout-vent length (SVL), measured from the center of the rostral to the posterior margin of the cloacal scale; (2) tail length, from the posterior margin of the cloacal scale to the distal tip of the terminal scale; (3) head length, from the center of the rostral tip to the corner of the mouth, ventrally; (4) head width, measured at the suture of the supralabials with the infralabials; (5) internasal length; (6) parietal length; (7) posterior temporal scale counts; (8) supralabial scale counts; (9) infralabial scale counts; (10) infralabial scales contacting the anterior pair of chinshields; (11) ventral scale counts; (12) subcaudal scale counts; (13) tail tip coloration, ranging from fully black [1] to fully white [2]; (14) snout blotch shape, ranging from single [1] to divided [2]; (15) white nuchal collar length, dorsally; (16) black nuchal collar length, dorsally; (17) number of dark dorsal stripes; (18) number of paravertebral stripes, sensu Ferrarezzi (1993); (19) number of white dorsal stripes; (20) supralabial blotch cover, measured in supralabial scales covered. In order to account for allometry, morphometric values were log-transformed, categorical variables were coerced from character to numeric, and additional categories include ratios of the aforementioned meristic and morphometric values.

Our generated dataset combines discrete and continuous variables, which are presumed to have different distributions. To further ensure that our data adhered to model assumptions, we identified outliers, collinearity, zero-variance in characters, and possible problems in our dataset through the inspection of Quantile-Quantile plots, correlograms, histograms, and box plot graphs. In order to reduce multicollinearity, we filtered and removed variables with a high pairwise Pearson correlation index (> 0.8). We employed three multivariate approaches to data analysis: 1) Principal Component Analysis (PCA), as a dimensionality reduction technique in order to find the underlying structure of the morphological dataset by identifying patterns in the data and expressing it in a new, lower-dimensional space, as an exploratory approach to visually test for morphological differences among groups; 2) Partial Least Squares Discriminant Analysis (PLS-DA), a supervised discrimination method based on the combination of Partial Least Squares regression (which applies linear regression, principal component analysis, and correlation analysis to model the relationship between two matrices of data) to a Discriminant Analysis, leveraging the latent variables obtained from Partial Least Squares (PLS) to classify samples into predefined groups; 3) Discriminant Function Analysis (DFA), a linear regression technique, in order to classify observed specimens into predefined recognized species groups, and performed a Jackknife cross-validation test in order to generate an assignment matrix between observed individuals and their respective specific identity. Our application and assumption checks of PCAs follow Jolliffe & Cadima (2016), the PLS-DA follows Ruiz-Perez et al. (2020), and DFAs follow McLachlan (2004); for each analysis, we projected the first two components onto orthogonal axes for visualization with t-distributionbased ellipses (t = 0.95) for OTUs. Furthermore, we plotted DFA, PLS-DA, and PCA autovectors in order to evaluate individual variable contribution to variation distribution for the analyzed individuals. We employed the distribution-free, non-parametric analyses (PCA and PLS-DA) for the whole dataset (continuous, discrete, ratios) and the parametric analyses (DFA) for selected normally distributed variables (continuous). However, due to a small sample constraint, these multivariate analyses should be seen as a strictly preliminary step for testing species boundaries, constituting an approach to dimensionality reduction of variables, in order to provide a visualization of spatial congruence among the characters from our putative operational taxonomic units. We attempted to evaluated intraspecific presence of sexual dimorphism with a Student t-test (t) for morphometric (continuous) and a Wilcoxon signed-rank test (W) for meristic (discrete) characters, both with P-value = 0.05, after evaluating the assumptions of univariate normality by using a Shapiro-Wilk test, and

homoscedasticity through Levene's test (ZAR 1999). Considering the low number of available specimens of A. quirogai (4 males, 4 females), our exploratory analyses failed to assess sexual dimorphism in the species; it should be noted that most statistical analyses upon meristic and morphometric data require higher sample sizes (at least > 5 per category, as in the Wilcoxon test) (ZAR 1999). Ranges are reported in parentheses, followed by mean ± standard deviation, and sample size. Furthermore, pairwise correlation between some morphological characters was assessed between both sexes with a Pearson correlation test (ZAR 1999), which is available at Supplementary Figure 1. All statistical analyses were conducted using built-in functions in R Environment (R Core Team 2021), and custom scripts can be made available upon request to the senior author (OME-N).

We describe the skull morphology of A. quirogai (UFRGS 6676) based on a high-resolution micro-CT scan, performed with a Bruker SkyScan 1173 (Bruker, Kontich, Belgium) at the IPR/PUCRS in Brazil. The scan was recorded over a 180° rotation with a frame averaging of 2, an X-ray beam with 50 kV source voltage, 160 µA current, and an exposure time of 800 ms per projection, without the use of a filter. Rotation steps of 0.33° degrees were used, resulting in 727 projections, an isotropic voxel size of 7.86 µm, and a total scan duration of 38:40 min. We reconstructed the CT-dataset using N-Recon software version 1.7.4.6 (Bruker MicroCT, Kontich, Belgium) and rendered the images in three dimensions through the aid of Amira visualization software (FEI, Thermo Fisher Scientific). Segmentation to separate and color the bones was also performed using Amira. We use the osteological terminology of Bullock & Tanner (1966) and Cundall & IRISH (2008), and the description of the skull follows En-TIAUSPE-NETO et al. (2020a, 2021b). We compared the skull of A. quirogai with all available descriptions of Elapomorphini skulls: *Apostolepis ambiniger* (Peters, 1869), *Aposto*lepis albicollaris Lema, 2002, A. assimilis, A. cearensis, and A. sanctaeritae (Ferrarezzi et al. 2005, Entiauspe-Neto et al. 2020, 2021a, 2021b, 2021d, 2022).

Molecular phylogenetic analyses

We extracted DNA from muscle tissue using the DNeasy DNA Extraction kit (Thermo Fisher, MA, USA). We generated sequence data for a new specimen of *A. quirogai*, targeting the mitochondrial genes 12S rRNA (12S ribosomal RNA), 16S rRNA (16S ribosomal RNA), cytb (Cytochrome B), and coxI (Cytochrome c oxidase subunit 1), and the nuclear genes bdnf (Brain-derived neurotrophic factor), cmos (Oocyte maturation factor Mos), and nt3 (Neurotrophin-3). Sequence fragments for seven genes were amplified via polymerase chain reaction (PCR). Primers are described in Supplementary Table 1. PCRs were performed using standard protocols, with addition of 0.4% of Triton X 100 to increase the efficiency of amplification. We used an annealing temperature of 54 °C for 12S rRNA and 16S

rRNA, 56 °C for bdnf, a touchdown cycle of 50–60 °C, with final annealing of 54 °C for cytb, nt3 and cmos. PCR products were purified with shrimp alkaline phosphatase and exonuclease I (GE healthcare, Piscataway, NJ, USA), and the sequences were processed using the DYEnamic ET Dye Terminator Cycle Sequencing Kit in a MegaBACE 1000 automated sequencer (GE healthcare, Piscataway, NJ, USA) following manufacturer's protocols. Both strands were checked, and when necessary edited manually. The consensus of both strands was generated using Geneious software (v. 7.1.8., KEARSE et al. 2012).

The phylogenetic relationships of *A. quirogai* and other congeners were tested with an extended molecular data set for Caenophidia, modified from ZAHER et al. (2018), resulting in a total of eight gene fragments, 4,730 base pairs, and covering 88 terminals. This matrix is available in Supplementary File 2. Sequences were aligned using MAFFT 1.3.6 software (Катон et al. 2005) plugin in Geneious (v. 7.1.8., KEARSE et al. 2012). The gene fragments 12S rRNA and 16S rRNA were aligned with an E-INS-i algorithm, and other gene fragments with a G-INS-i algorithm. We employed default parameters for gap opening and extension. We visually checked protein-coding genes with Geneious to verify the correct reading frame. Mitochondrial and nuclear gene fragments were concatenated with SequenceMatrix (v. 1, VAIDYA et al. 2011). We considered parsimony-informative sites as areas in our alignment which contained at least two types of nucleotides, occurring with a minimum frequency and number of two, and were evaluated in the final alignment with a custom script on R Environment (v. 4.3, R Core Team 2021).

We used PartitionFinder (v. 2, Lanfear et al. 2016) to choose the combined sets of partitioning schemes and models of molecular evolution, based on the Akaike Information Criterion with correction (AICc). We treated the two rRNA genes (12S and 16S) as separate partitions and partitioned protein coding genes by codon positions. We used the greedy search option in PartitionFinder, allowing only the selection of models of molecular evolution implemented in RAxML 8.2.3 (Stamatakis 2014) without any correction for proportion of invariant sites, as recommended in the RAxML's manual. We also developed a modular automated Unix script for handling Nexus gene fragment alignments to generate a PartitionFinder file, which is also available at: https://github.com/omarentiauspe/partition-finder script.

We inferred phylogenetic relationships under a Maximum Likelihood (ML) framework, computed using RAxML software (Stamatakis 2014) in CIPRES Science Gateway (available at https://www.phylo.org/), with a mixed partition model from PartitionFinder 2, searching the most likely tree 100 times and conducting 1,000 nonparametric bootstrap replicates. The run was performed with the GTR + Γ model for all partitions. We consider a node support for bootstrap resampling as significant if it achieves a value equal or over 95% (Felsenstein & Kishino 1993). Uncorrected genetic distances (p-distances) were calculated for the 16S rRNA gene fragment using MEGA software

(v. 11, Tamura et al. 2021), using a d parameter (Transitions + Transversions), while assuming uniform rates among sites and a homogeneous pattern among lineages. The p-distance calculation was made based on the proportional (p) differences among nucleotide sites in which two compared sequences differ, as inferred through the division of nucleotide differences by the total nucleotides (Tamura et al. 2021). The ML topology was used to infer branch lengths and patristic distances (absolute time and mutation rate, to which patristic distances represent the sum of branch lengths used to link the terminal nodes of two species in a tree) as reinforcement proxies of genetic distance, following Montingelli et al. (2020) and Entiauspe-Neto et al. (2021c), inferred with the 'ape' package (Paradis & Schliep 2019), in R environment (v. 4.3, R Core Team 2021).

Within the A. assimilis species group, we generated a list of putative morphological synapomorphic characters, modified from FERRAREZZI et al. (2005), and evaluated over the morphological phylogeny with YBYRÁ software (MACHADO 2015), using TNT (GOLOBOFF et al. 2008) script applications in Python language. The list of putative synapomorphies and coded characters are available at Supplementary Material 2–4. In order to explore the character optimization of two closely related species, A. arenaria and A. gaboi, these taxa are included in the ML topology as a sister clade to A. cearensis, as suggested by Ferrarezzi et al. (2005). YBYRÁ categorizes character transformation events from any source of data given all possible optimization schemes in a set of trees. It proceeds by spawning trees and data matrix to TNT to compile synapomorphies using TNT's command "-apo". Morphological characterstate transformations of a node were considered synapomorphies if they were optimized unambiguously (without arbitrary selection of accelerated, ACCTRAN, or delayed optimization, DELTRAN). YBYRÁ generates color-coded boxes to indicate if a synapomorphic character-state occurs only in the clade in question (non-homoplastic) or also occurs in other clades (homoplastic), and if it is shared by all terminals of the clade (unique) or is subsequently transformed into one or more different states within the clade (non-unique) (MACHADO 2015).

Results

Morphological based species determination

Our exploratory multivariate analyses (PCA, PLS-DA, DFA) revealed a broad overlap of morphological variation among the analyzed OTUs (top, females and males; middle, males; bottom, females; Fig. 1). Our PCA analysis with female and male specimens is recovered with a major overlap of clustered individuals, belonging to *Apostolepis assimilis*, *A. cearensis*, *A. cf. quirogai*, and *A. quirogai*. Specimens of *A. cf. quirogai* and *A. quirogai* are recovered closely in PCA analyses separated by sex, although our limited sampling precluded the evaluation of variation within individual female and male categories. Our PLS-DA analyses recover clustered individuals of *A. cf. quirogai* and *A. quirogai* for

the female (F) and males and females (M+F) subsets. As for the DFA analyses, specimens of A. cf. quirogai and A. quirogai are recovered closely in all subsets (M+F, M, and F). The Jackknife cross-validation test using males and females assigned 40% of A. cf. quirogai specimens to A. quirogai, and 66.6% of A. quirogai to A. cf. quirogai, which demonstrates a high similarity between both entities. Based on the PCA, PLS-DA, and DFA analyses outputs, the Jackknife cross-validation test, and an overlap of diagnostic characters proposed by GIRAUDO & SCROCCHI (1998) (ventrals over 260, wide dorsolateral stripes, black venter), we confirm the identification of these specimens as A. quirogai.

Phylogenetic relationships of Elapomorphini taxa

Our phylogenetic tree inferred using maximum likelihood (ML; Lnl = -71666.809566) based on concatenated nuclear and mitochondrial gene fragments, recover the genera Apostolepis, Elapomorphus, and Phalotris as reciprocally monophyletic with significant support (Fig. 2, Supplementary Files 4–5, bootstrap support = 100%). Inferred best-fit partitions and models for PartitionFinder 2 concatenated ML analysis can be seen in Supplementary Tables 2-3. As for parsimony informative sites, we recovered an average of 415.0 bp (median value = 312) for the mitochondrial locus and 245.6 bp (median value = 265) for our nuclear partitions. Our results differ from the previous phylogenetic hypotheses of Zaher et al. (2018, 2019) and OLIVEIRA et al. (2023), who recover Phalotris as a sister group to Elapomorphus and Apostolepis, and rather support a relationship of *Apostolepis* as a sister group to *Elapo*morphus and Phalotris. The P. mertensi specimen from ZAHER et al. (2019) is shown to be a chimeric individual comprised of two species, with the 12S rRNA sequence of P. mertensi (JQ598826.1) having 334 identical sites (100%) site match) to P. nasutus (GQ457818.1), being herein reidentified as a duplicate sequence of P. nasutus. All Elapomorphini genera are recovered with a clade of Echinantherini, Philodryadini, Tachymenini, and Pseudoboini as a sister group, in accordance with previous phylogenetic arrangements supporting a monophyletic Xenodontinae Cope, 1895 subfamily (ZAHER et al. 2018, ENTIAUSPE-NE-To et al. 2022; Supplementary File 6). Surprisingly, we recover A. quirogai firmly nested with other terminals of the A. assimilis species group, as a sister species to A. assimilis (bootstrap support = 100%). We also recover the *Phalotris* tricolor species group (sensu Ferrarezzi 1993 and Lema et al. 2005) as polyphyletic in our ML analysis, with Phalotris mertensi Hoge, 1955 as a sister species to a clade of Phalotris nasutus (Gomes, 1915), and Phalotris lativittatus FERRAREZZI, 1993. Sampled terminals from the *P. bilinea*tus and P. nasutus species groups (sensu Ferrarezzi 1993) are also recovered as monophyletic. We recover all sampled terminals from the A. dimidiata species group (sensu Ferrarezzi 1993) as monophyletic in the ML analysis. The Apostolepis flavotorquata species group had only a single

sequenced terminal (*Apostolepis flavotorquata* [Duméril, Bibrón & Duméril, 1854]), and could not be verified for its reciprocal monophyly. In order to maintain the *A. assimilis* species group as monophyletic, we propose the inclusion of *A. quirogai*, and provide an update to its diagnosis below. Although no molecular samples are available yet

for *A. arenaria* and *A. gaboi*, we tentatively include these species in the *A. assimilis* group, considering these species as fitting in the proposed morphological diagnosis of the group. Nonetheless, further phylogenetic analyses based upon molecular or morphological data are needed to verify their relationships to other congeners.

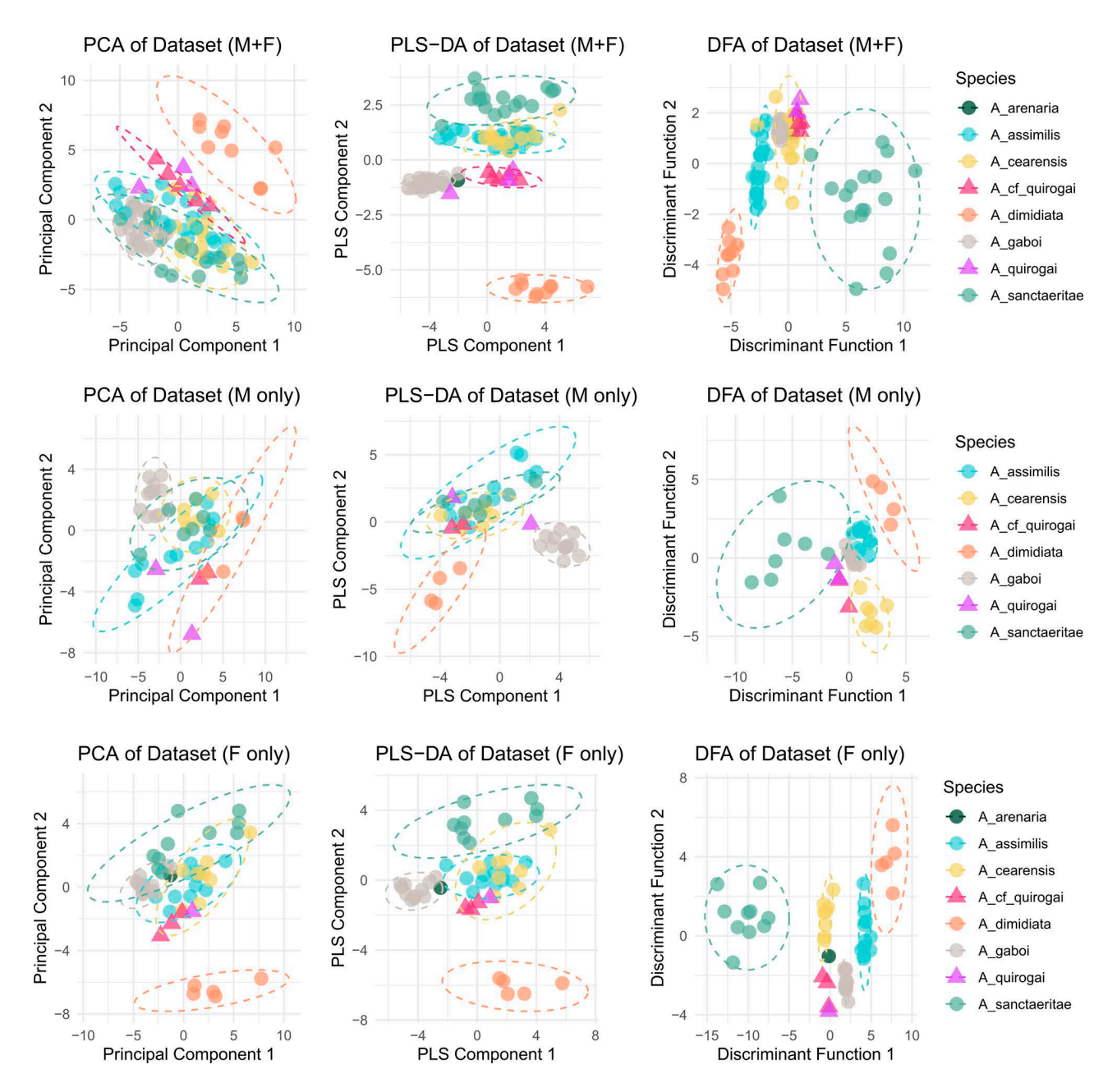


Figure 1. Bidimensional scatterplots showing the results from the multivariate analyses inferred over a dataset of *Apostolepis* species from the *A. assimilis* group and selected outgroup (*A. dimidiata*). On the left, the first two PC components of Principal Component Analyses (PCA). In the middle, the first two PLS components of the Partial Least Squares Discriminant Analysis (PLS-DA). On the right, the first two discriminant functions of Discriminant Function Analyses (DFA). Analyses are separated by partitions containing both sexes (M+F, top), only males (M, middle), and only females (F, bottom). Non-parametric (PCA and PLS-DA) analyses are based on the whole dataset (continuous, discrete, and ratio of variables), and parametric (DFA) analyses are based on the normally distributed dataset (continuous variables). Specimens identified herein as *A. quirogai* are represented as triangles, and new specimens recorded and tested in this study are referred to as *A. cf. quirogai*.

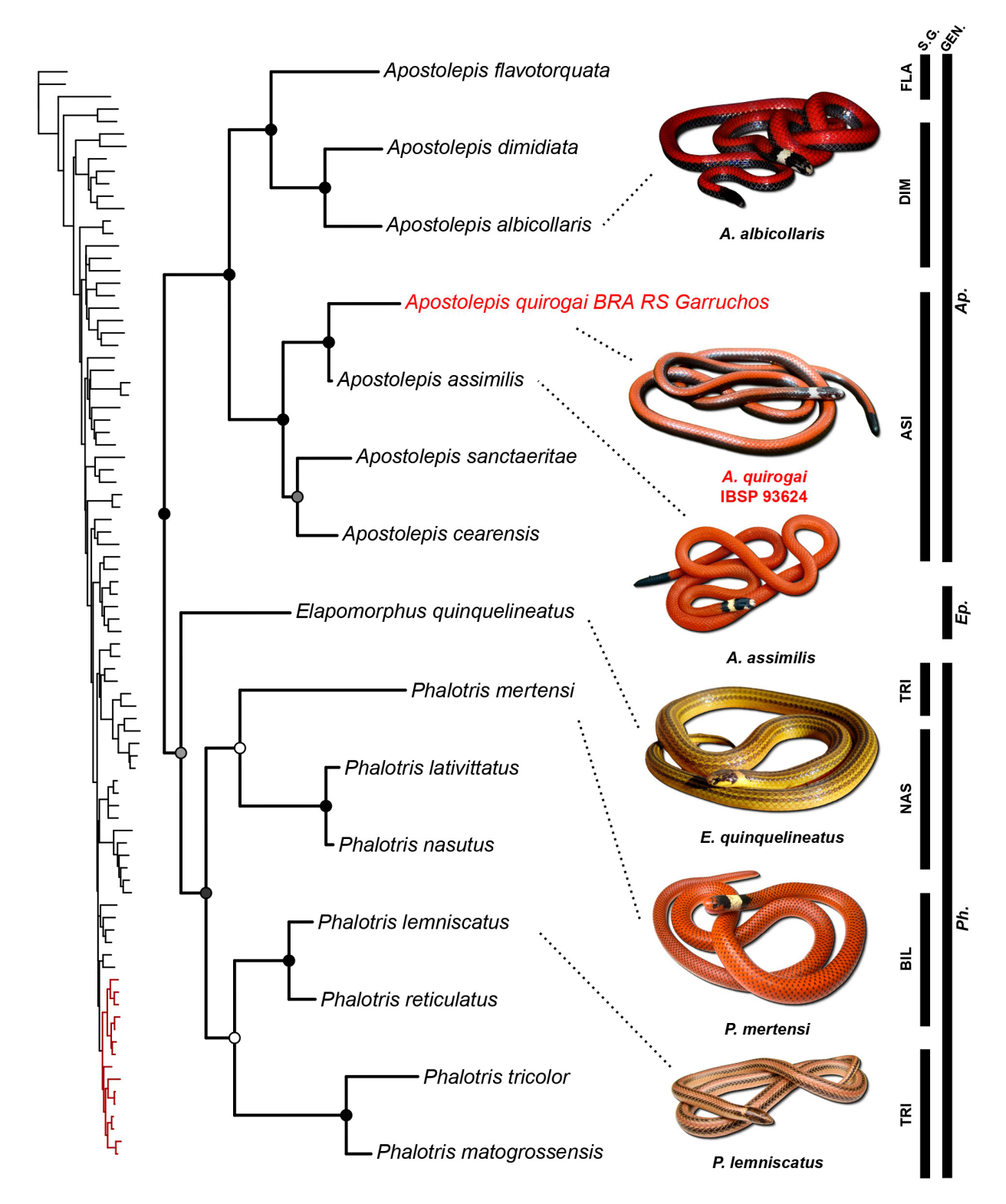


Figure 2. Phylogenetic relationships of sampled Elapomorphini genera (*Apostolepis*, *Elapomorphus*, *Phalotris*), from seven concatenated nuclear and mitochondrial DNA gene fragments, as inferred by a Maximum Likelihood (RAxML) framework. Elapomorphini tribe is indicated as dark red in Caenophidia topology (left). Node labels are: white (≥ 70% bootstrap support); gray (< 70% bootstrap support); black (100% bootstrap support). Legend: S.G. = Species groups; GEN = Genera; FLA = *A. flavotorquata* species group; DIM = *A. dimidiata* species group; ASI = *A. assimilis* species group; TRI = *P. tricolor* species group; NAS = *P. nasutus* species group; BIL = *P. bilineatus* species group. Photograph credits: Cyro de Sousa Bernardes (*A. albicollaris*), Marcelo Duarte (*A. quirogai*), Laurie Vitt (*A. assimilis*), Pedro H. Martins (*E. quinquelineatus*), OMAR M. Entiauspe-Neto (*P. mertensi*), Márcio Borges-Martins (*P. lemniscatus*).

Definition of the *Apostolepis assimilis* species group

Diagnosis: Small to medium-sized snakes; preocular present, separated from nasal; fourth and fifth supralabials contacting parietal or posterior temporal; infralabials 7-8, with first four contacting anterior pair of chinshields; temporals 0+1; ventrals from 163 to 287; terminal scale with a sharply pointed edge; large white blotch on snout, undivided, covering the rostral, internasals, and reaching the frontal shield; moderate to large black and white nuchal collars (2-5 scale rows); dorsal background color uniformly red, orange, or tan; black dorsal stripes absent or present, ranging from two wide lateral stripes (3-5 scale rows each) to five thin dorsal stripes (1 scale row each); uniformly black or white ventral surface; gular region ranging from white to uniformly black; terminal shield black, undifferentiated from the tail tip coloration; Duvernoy's gland moderately developed; harderian gland well developed, reaching the temporal region; adductor jaw muscles moderately developed, reaching the dorsal surface of the brain case.

Distribution: Members of the *A. assimilis* species group occur from northeastern to southern Brazil, Argentina, and Paraguay. Widely distributed across the Caatinga and Cerrado, with sparse portions of their range in the Atlantic Forest and Uruguayan Savannas.

Content: A. arenaria Rodrigues, 1993 (this study), A. assimilis (Reinhardt, 1861), A. cearensis Gomes, 1915, A. gaboi Rodrigues, 1993 (this study), A. sanctaeritae Werner, 1924, and A. quirogai Giraudo & Scrocchi, 1998 (this study) (Fig. 3).

Apostolepis quirogai GIRAUDO & SCROCCHI, 1998 (Figs. 2-7)

Synonymy: *Apostolepis quirogai* GIRAUDO & SCROCCHI, 1998. Holotype FML 6000 (adult female), from Posadas (-27.365077° S, -55.923487° W, 120 m altitude), Misiones, Argentina; paratype FML 6001 (adult male), same locality. Lema & Cappellari 2001: 121, Lema 2001: 31, Lema et al. 2004: 67, Ferrarezzi et al. 2005: 217, Santos et al. 2018: 2, Entiauspe-Neto et al. 2019: 75, Entiauspe-Neto et al. 2020: 341, Entiauspe-Neto et al. 2021a: 127, Entiauspe-Neto et al. 2021b: 235, Entiauspe-Neto et al. 2022: 154.

New material: We report five new specimens from Argentina and Brazil. Adult female (LGE 1771) from Garupá (-27.455901° S, -55.861002° W), Misiones, Argentina; juvenile male (UFRGS 5668) from Eugênio de Castro (-28.526822° S, -54.150768° W), Rio Grande do Sul, Brazil; adult male (IBSP 93624) from Garruchos (-28.191112° S, -55.637373° W), Rio Grande do Sul, Brazil; adult female

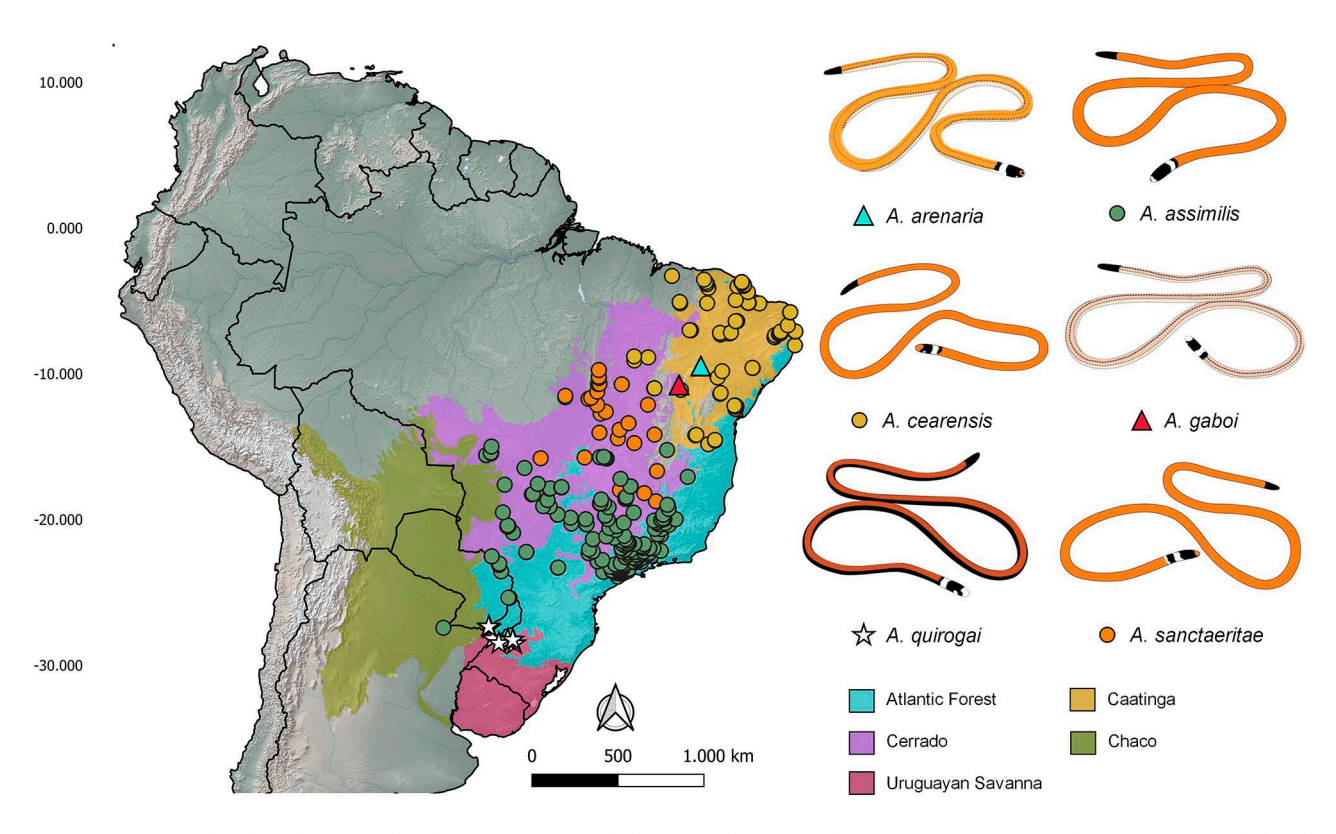
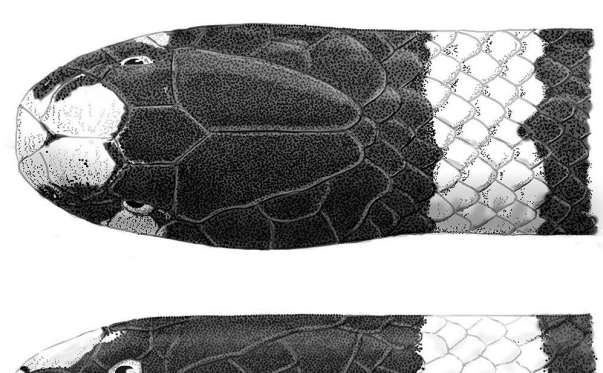


Figure 3. Geographic distribution and coloration pattern of the *Apostolepis assimilis* species group in South America, as redefined in this work, based on verified point-records from this work and Entiauspe-Neto et al. (2021a, 2022). Ecoregions modified from Olson et al. (2001).

-54.617067° W), Rio Grande do Sul, Brazil; adult female (UFRGS 7834) from Santo Antônio das Missões (-28.508860° S, -55.225757° W) Rio Grande do Sul, Brazil; adult female (UFRGS 6676) from Mato Queimado (-28.256607° S, -54.616643° W), Rio Grande do Sul, Brazil.

Diagnosis: This species has (1) 15/15/15 dorsal scales; (2) preocular present, separated from nasal; (3) loreal absent; (4) temporals 0+1; (5) supralabials six, 2nd-3rd in contact with orbit; (6) infralabials seven or eight, 1st-4th in contact with anterior chinshields; (7) ventrals 245-287 (in males 245-279; in females 268-287); (8) subcaudals 23-30 (in males 23-30; in females 24-27); (9) dorsal pattern uniformly red, with two large lateral black stripes, rostral blotch white and large; (10) ventral pattern uniformly black, with white coloration coalescing outwards from center of ventral scales towards its edges, white gular region; (11) white nuchal collar present, 3-4 scales wide, black nuchal collar present, 1.5-3 scales wide; (12) caudal blotch 6-8 scales long on dorsum, 3-5 on venter, terminal scale black; (13) supralabial blotch medium sized, two scales wide; (14) SVL 190-435 mm (in females 212-435 mm, in males 190-410 mm); (15) TL 15-34 mm (in females 15-30 mm, in males 19-34 mm); (16) dentary teeth 8–9; (17) pterygoid teeth four; (18) palatine teeth 4-5; (19) parietal bone does not contact parasphenoid bone rostrum; (20) small lateral wings on ascending process of premaxilla; (21) frontal edge of nasals straight. In our parsimony-based character optimization, A. quirogai is recovered with the following unambiguous, non-private autapomorphies within the A. assimilis species group: lower mean range of subcaudals, 23-26 or fewer in females, 23-31 or fewer in males [character state: 14(2)]; conspicuously curved dentary bone [character state: 17(1)]; prearticular crest of compound bone same height as surangular crest [character state: 18(1)].

Redescription: We provide a redescription based on an adult female (UFRGS 6676, Fig. 3) specimen from Mato Queimado, Rio Grande do Sul, Brazil. Total length 381 mm (holotype: 228 mm); SVL 356 mm (holotype: 212.5 mm); tail length 25 mm (6.3% of total length; 7.5% of SVL; holotype: 15.5 mm). Head length 6.00 mm (1.52% of total length; 1.82% of SVL; holotype: 7.3 mm); head width 3.43 mm (57.7% of head length; holotype: 3.27 mm); interorbital distance 2.40 mm (69.9% of head width); rostro-orbital distance 3.11 mm (51.83% of head length); naso-orbital distance 0.90 mm (15% of head length). Cervical constriction indistinct. Head well distinct from neck, rounded in dorsal view, arched in lateral view. Pupil sub-elliptical. Rostral rounded in dorsal view, not projected in lateral view, 1.03 mm wide, length of portion visible in dorsal view slightly smaller than a third of internasal length. Internasals paired, rectangular, 1.86 mm long, 1.30 mm wide; each internasal contacts rostral, nasal, preocular, supraocular, and frontal. Prefrontals absent, likely fused to internasals. Frontal hexagonal, 2.15 mm long, 1.76 mm wide, contacting internasals, supraoculars, and parietals. Supraocular trapezoidal, longer than wider, in contact with posterior edge of prefrontal, lateral edge of frontal, superior edge of preocular, superior edge of postocular, and anterior edge of parietal. Parietals paired, rectangular shaped; right parietal 3.45 mm long (57.50% of head length), 1.90 mm at its largest width (55.39% of head width), contacting frontal, supraocular, postocular, fourth and fifth supralabials, anterior temporal, occipital, and interoccipitals. Occipitals square-shaped, enlarged; each occipital contacts a single interoccipital and dorsals. Interoccipitals three, slightly smaller than vertebral and paravertebral rows of dorsals. Nasal triangular, undivided, longer than wide, well separated from preocular; contacting rostral, internasals, first and second supralabials. Preocular pentagonal, as wide as high. Postocular pentagonal, contacting third through fifth supralabials, supraocular and parietal. Temporals o+1, contacting fifth and sixth supralabial, latero-posterior edge of parietal, dorsals, and a single interoccipital. Six supralabials, 2-3 entering orbit; first contacting nasal, second contacting nasal and preocular, third and fourth contacting postocular, fourth and fifth contacting postocular and parietal, sixth well separated from parietal by temporal; fifth supralabials largest in height. Mental triangular, as long as wide. Two pairs of chinshields, second pair longer. Seven infralabials, 1-4 in contact with anterior chinshields, 5-7 in contact with posterior chinshields, first pair in contact with each other behind mental; fourth and fifth infralabials largest, equal in size. Dorsals smooth, in 15/15/15 rows. Pre-cloacal scale divided. Ventrals 267; pre-





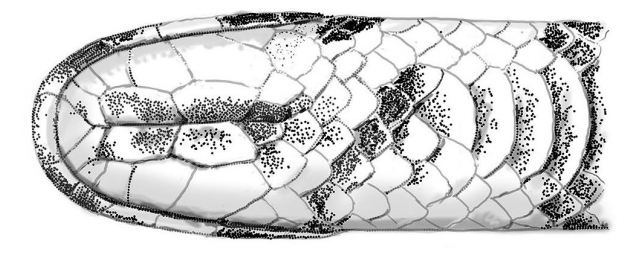


Figure 4. Head pholidosis of *Apostolepis quirogai* (UFRGS 6676) from Mato Queimado, Rio Grande do Sul, Brazil. Dorsal (top), lateral (middle), and ventral (bottom) surface views.

Table 1. Meristic and morphometric variation for selected informative and variable characters in *Apostolepis quirogai*. Holotype is indicated with a cross (\dagger), and paratype is indicated with an asterisk (*). Measurements are given in millimeters (mm). SVL = snoutvent length; TL = tail length; \circlearrowleft = male; \circlearrowleft = female. We report five new specimens from Argentina and Brazil, highlighted in bold.

Voucher	Sex	SVL	Tail length	Head length	Total length	Ventrals	Subcaudals	Supralabials (R)	Supralabials (L)	Infralabials (R)	Infralabials (L)
UFRGS 6676	2	330	25	6	355	267	27	6	6	7	7
LGE 1771	2	435	30	6.5	465	287	26	6	6	8	8
UFRGS 7834	2	315	23	5	338	268	24	6	6	7	7
FML 6000 †	9	212	15	7.3	227	276	24	6	6	8	8
IBSP 93624	3	410	23	7.3	433	279	23	6	6	7	7
FML 6001 *	3	365	30	9	395	269	29	6	6	8	8
MCP 12185	8	397	34	12	431	267	28	6	6	7	7
UFRGS 5668	8	190	19	5	209	245	30	6	6	7	7

ventrals four. Subcaudals paired, 27/27. Terminal scale pointed and acuminate, curved ventrally.

In preservative, head background coloration uniformly dark brown. White snout blotch single, covering rostral, nasals, internasals, and reaching up to frontal scale. Rostral background coloration uniformly dark brown on dorsal and ventral surfaces, with diffuse white pigmentation on its lateral edges. Lateral head surface uniformly dark brown. Supralabial blotch white, single and triangular shaped, covering half of second and third supralabials. White nuchal collar present, covering one scale at the two rows adjacent to the vertebral row, and up to three rows laterally. Black nuchal collar present, covering up to three rows, indistinct from the dorsolateral black bands. Diffuse dark brown pigmentation on outer edges of chinshields. Infralabials immaculate cream. Dark gular collar absent, with irregular dark brown pigmentation on gular scales. Dorsal background coloration light tan, without vertebral stripes. Two dorsolateral black stripes present, starting after white nuchal collar and reaching up to five dorsal rows. Ventral and subcaudal background coloration black, with white pigmentation coalescing from the central surface and inner margin of ventral scales to their outermost borders. Caudal blotch dark brown, small sized, covering up to five scale rows on dorsum, indistinct from dorsolateral black stripes laterally, and three subcaudal scales ventrally.

Coloration in life description based on adult male (IBSP 93624) from Garruchos and adult female (UFRGS 6676) from Mato Queimado, both from Rio Grande do Sul, Brazil (Figs 5–7). Head background coloration uniformly black. White snout blotch entire, covering rostral, nasals, internasals, reaching up to frontal scale. Rostral background coloration uniformly black on dorsal and ventral surfaces, with diffuse white pigmentation on its lateral edges. Lateral head surface uniformly black. Supralabial blotch white, single, and triangular shaped, covering half of second and third supralabials. White nuchal collar present, covering one scale at the two rows adjacent to the vertebral row, and up to three rows laterally. Black nuchal collar present, covering up to three rows, indistinct from the dorsolateral black bands. Diffuse dark brown pigmenta-

tion on outer edges of chinshields. Infralabials immaculate cream. Dark gular collar absent, with irregular dark brown pigmentation on gular scales. Dorsal background coloration bright red, without vertebral stripes. Two black dorsolateral stripes present, starting after white nuchal collar and reaching up to five dorsal scale rows. Ventral and subcaudal background coloration black, with white pigmentation coalescing from the central surface and inner margin of ventral scales to their outermost borders. Caudal blotch black, small sized, covering up to five scale rows on dorsum, indistinct from black dorsolateral stripes laterally, and up to three subcaudal scales ventrally.

Selected informative characters for variation are provided in Figure 8 and Supplementary Figure 2. While no sexual dimorphism was detected in this species, it should be noted that a marked pattern appears in subcaudal scale numbers (Supplementary Fig. 1), and our results likely should be seen as provisional, due to sample constraints. From the examined series, snout-vent length ranges from 190-435 mm (331.75 ± 90.12, N = 8), in females 212-435 mm $(323 \pm 91.24, N = 4)$ and males $190-410 \text{ mm} (340.5 \pm 120,$ N = 4). Tail length ranges from 15–34 mm (24.87 \pm 6.26, N = 8), in females 15–30 mm (23.25 \pm 6.23, N = 4) and males 19– 34 mm (26.5 \pm 6.75, N = 4). Total length ranges from 209– 465 mm (356 \pm 95.2, N = 8), in females 227–465 mm (346 \pm 97, N = 4) and males 209–433 mm (367 \pm 106, N = 4). Head length ranges from 5.0-12 mm (7 \pm 2.32, N = 8), in females 5.0-7.3 mm (6.2 ± 0.9, N = 4) and males 5.0-12 mm (8.32 ± 2.94, N = 4). Ventrals range from 245–287 (269 \pm 12, N = 8), in females 268-287 (274 \pm 9.2, N = 4) and males 245-279



Figure 5. Overview of *Apostolepis quirogai* coloration in life, in dorsal (top), dorsolateral (middle), and ventral (bottom) views.

(265 \pm 14, N = 4). Subcaudals range from 23–30 (26 \pm 2.5, N = 8), in females 24–27 (25 \pm 1.5, N = 4) and males 23–30 (27 \pm 3.1, N = 4). One specimen (IBSP 93624) has anomalous temporal scales (1+ 0+ 1) on both sides of its head.

Comparisons: In this section, characters from other species are presented in parentheses. *Apostolepis quirogai* bears a unique combination of external morphology characters and a restricted geographic range, which should as-

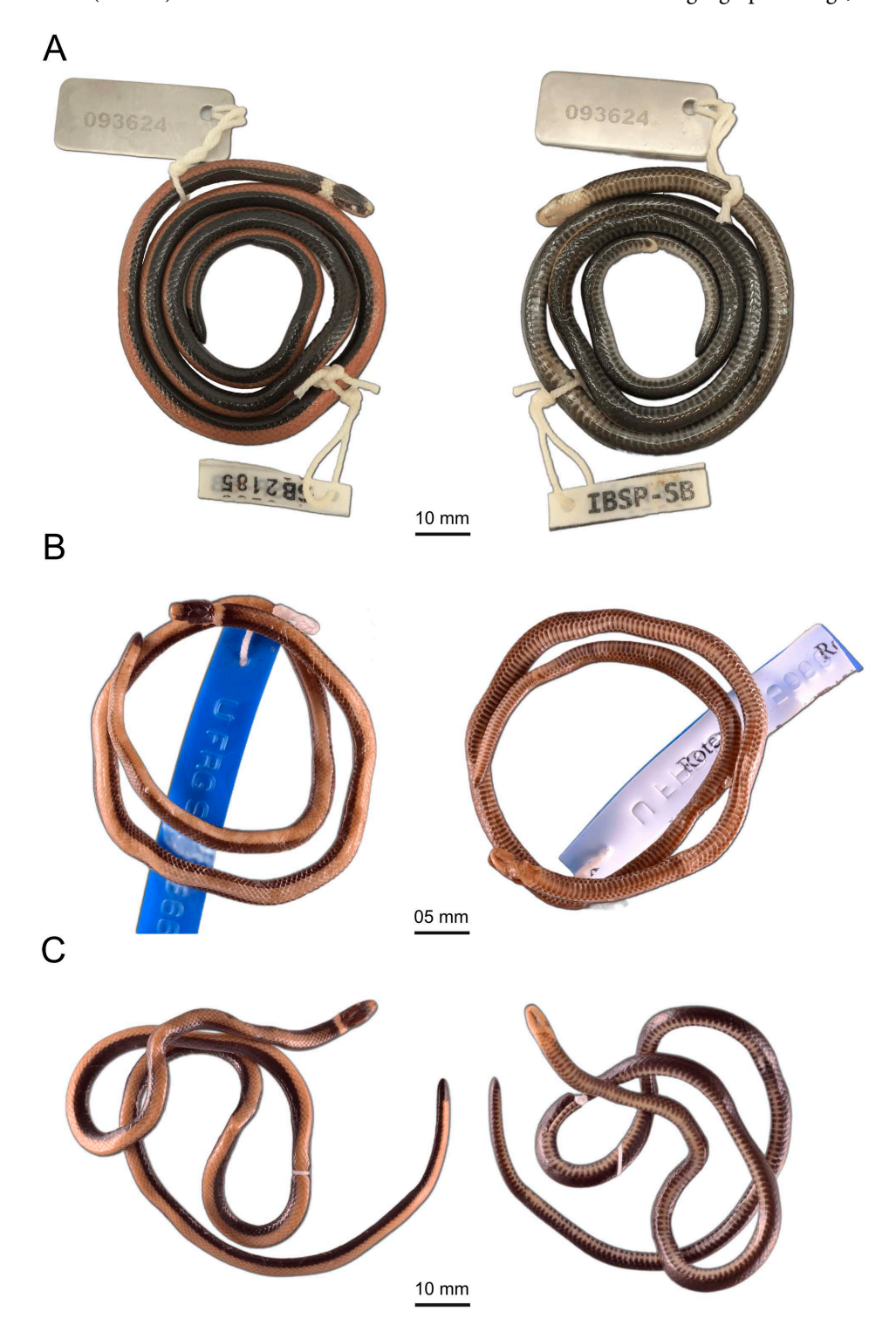


Figure 6. Overview of selected new specimens of *Apostolepis quirogai* in dorsal (left) and ventral (right) views. (A) Adult male (IBSP 93624) from Garruchos, Rio Grande do Sul, Brazil; (B) juvenile male (UFRGS 5668) from Eugênio de Castro, Rio Grande do Sul, Brazil; (C) adult female (UFRGS 6676) from Mato Queimado, Rio Grande do Sul, Brazil.

sist in unambiguously identifying it (Table 2). Nonetheless, two species might possibly be confused with *A. quirogai*, whether in the field due to its sympatric occurrence with a similarly colored congener, or in scientific collections, should specimens lack clear geographic provenance. These two species are *A. albicollaris* and *A. dimidiata*, which will be addressed in detail below.

Apostolepis quirogai is known to occur in sympatry with A. dimidiata, another red species of Apostolepis that occurs in the Uruguayan Savanna. Both species share two wide black dorsolateral stripes, a red dorsal background coloration, and a black venter, although the latter character is known to be polymorphic in A. dimidiata (ENTIAUSPE-NETO et al. 2019). Apostolepis quirogai can be readily distin-







Figure 7. Coloration in life of *Apostolepis quirogai* specimens. (A) Dorsal view, adult male (IBSP 93624) from Garruchos, Rio Grande do Sul, Brazil; (B) dorsal view, juvenile male individual (unvouchered) from Posadas, Misiones, Argentina; (C) ventral view, same previous individual. Photograph credits: MARCELO DUARTE (A), ARIEL LOPEZ (B-C).

guished from this congener by having a white nuchal collar (absent), a wide snout blotch (absent), a smaller white supralabial blotch (supralabial blotch larger, trapezoidal, covering up to five scales), temporals 0+1 (temporals absent), pointed terminal scale (rounded), and higher number of ventrals (226–240 in males, 220–244 in females).

While A. quirogai is restricted to the Uruguayan Savanna of southern Brazil and northeastern Argentina, its congener A. albicollaris, from the Cerrado of central Brazil, bears a strikingly similar coloration, which could render identification in museums problematic should the specimens lack geographic occurrence data. Both species share two wide black dorsolateral stripes, a red dorsal background coloration, white and black nuchal collars, a black venter, and have overlapping counts of supralabial and infralabial scales. Apostolepis quirogai can be distinguished from this congener by having an entire white snout blotch (divided), a smaller white supralabial blotch (supralabial blotch larger, trapezoidal, covering up to five scales), temporals o+1 (temporals absent), higher number of ventrals (196-208 in males, 206-230 in females), and a preocular scale separated from nasal (preocular contacting nasal).

Other species of the A. assimilis group (A. assimilis, A. cearensis, A. gaboi, and A. sanctaeritae) share several similarities with A. quirogai, such as a preocular present and separated from nasal, the fourth and fifth supralabials contacting parietal or posterior temporal, infralabials 7–8, with first four contacting anterior pair of chinshields, temporals o+1, terminal scale with a sharply pointed edge, large white snout blotch, undivided, covering the rostral, internasals and reaching the frontal shield, and moderate to large black and white nuchal collars (2-5 scale rows). Apostolepis quirogai can be readily distinguished from A. assimilis, A. cearensis, and A. sanctaeritae by having two wide black dorsolateral stripes (dorsal pattern uniformly red or orange) and a black venter (uniformly red or orange in A. assimilis and A. sanctaeritae, uniformly white in A. cearensis). From A. gaboi, it can be distinguished by having a red dorsal background coloration (tan or orange), and two dorsolateral stripes (five dorsal stripes). Most species of the assimilis group occur exclusively in the South American Dry Diagonal, with A. cearensis and A. gaboi restricted to the Caatinga of northeastern Brazil, and A. sanctaeritae restricted to the Cerrado of central and northeastern Brazil.

Another rare species, *Apostolepis tenuis* RUTHVEN, 1927, which occurs in the Humid Chaco and Cerrado of Bolivia, bears external morphological similarities to *A. quirogai*. Both species share wide black dorsolateral stripes, a very thin and long body, a small black tail tip, a wide white nuchal collar, a wide white snout blotch, and a high ventral scale count (245 in the known male, 265 in the known female). However, *A. quirogai* can be distinguished from *A. tenuis* by having a black venter (white or cream), a black terminal scale (white), higher infralabial count (5–6), and by lacking a vertebral stripe (black vertebral band present, up to three rows wide).

From Apostolepis dorbignyi (SCHLEGEL, 1837) and Apostolepis multicincta HARVEY, 1999, two extralimital species from the Argentine and Bolivian Dry Chaco, A. quirogai can be distinguished based on its black dorsolateral stripes (uniformly red dorsum), black venter (uniformly cream), and a black tail tip (uniformly white or cream). From another extralimital species, A. flavotorquata from the Cerrado of central Brazil, A. quirogai can also be distin-

guished based on its black dorsolateral stripes (uniformly orange dorsum) and black venter (uniformly yellow).

Furthermore, A. quirogai can be distinguished from Apostolepis adhara França, Barbo, Silva-Jr, Silva & Zaher, 2018, A. ambiniger, A. arenaria, Apostolepis borelli Peracca, 1904, Apostolepis breviceps Harvey, Gonzales & Scrocchi, 2001, Apostolepis christineae Lema, 2002, Apostolepis goiasensis Prado, 1942, Apostolepis intermedia

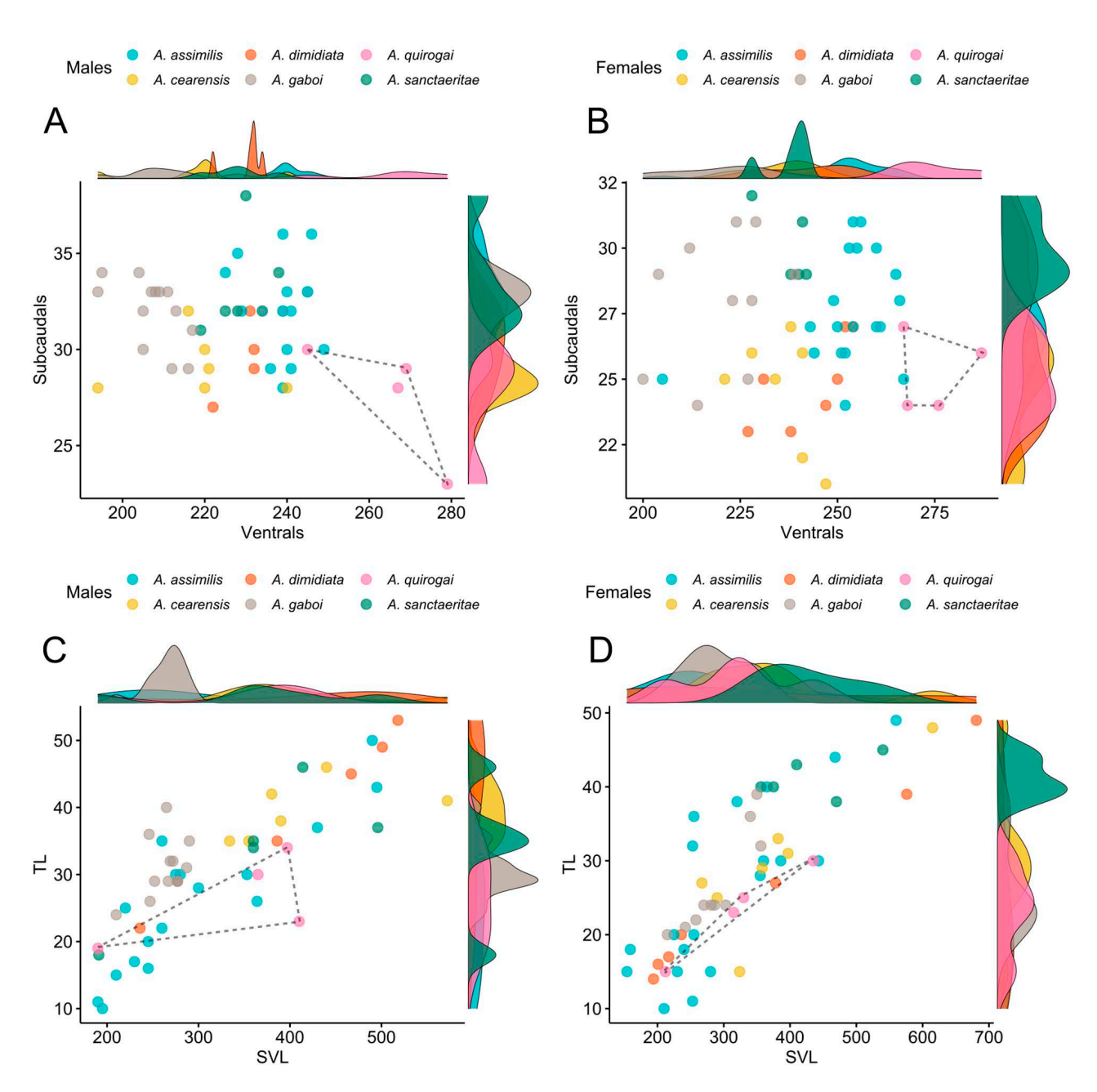


Figure 8. Overview of selected continuous and discrete morphological variation for selected *Apostolepis* species of the *assimilis* group (*A. assimilis*, *A. cearensis*, *A. gaboi*, *A. sanctaeritae*, *A. quirogai*) and *dimidiata* group (*A. dimidiata*), in scatter plot (inset) and density plot (margin) visualizations. (A) ventrals and subcaudals for males; (B) ventrals and subcaudals for females; (C) snout–vent length and tail length for males; (D) snout–vent length and tail length for females. The known variation of *A. quirogai* is displayed inside a minimum convex polygon.

OMAR M. ENTIAUSPE-NETO et al.

Table 2. Morphological comparison among *Apostolepis* species of the *assimilis* group, measurements are given in millimeters (mm). The species *A. arenaria* is not included due to the lack of available data, and will be individually addressed in another study by the authors. SVL = snout–vent length; TL = tail length; $\vec{\circlearrowleft}$ = male; $\vec{\circlearrowleft}$ = female.

	A. assimilis	A. cearensis	A. gaboi	A. sanctaeritae	A. quirogai	
SVL	140-780	180-635	210-490	190-686	190–435	
TL	10-55	10-59	18-40	18-64	15-34	
Head color	Black	Black	Black	Black	Black	
Light snout blotch	Present; undivided, large, white	Present; undivided, medium, orange	Present; undivided, large, white	Present; undivided, large, orange	Present; undivided, large, white	
Supralabial blotch	Large, single, over 3 rd to 5 th supralabial	Small or absent, single, over 4 th to 5 th supralabial	Large, single, over 3 rd to 5 th supralabial	Large, single, over 3 rd to 5 th supralabial	Large, single, over 3 rd to 5 th supralabial	
Light nuchal collar	Present, single, large (up to four rows)	Present, single, large (up to four rows)	Present, single, large (up to five rows)	Present, two, large (up to five rows in first, three in second)	Present, single, large (up to four rows)	
Black nuchal collar	Present, medium (up to four rows)	Present, medium (up to four rows)	Present, medium (up to three rows)	Present, large (up to seven rows)	Present, medium (up to three rows)	
Gular color	Immaculate cream	Immaculate cream or black	Black	Black	Immaculate cream	
Dorsal background color	Orange or red	Orange or red	Tan or light orange	Orange or red	Red	
Dorsal stripes	Absent	Absent	Present, five	Absent	Present, two	
Widest dorsal stripe size	Absent	Absent	One row	Absent	Five rows	
Ventral color	Immaculate cream	Immaculate cream or light orange	Immaculate cream	Orange	Black, with white pigmentation on center of ventrals	
Tail black blotch	Present, large, visible in dorsal and ventral views	Present, large, visible in dorsal and ventral views	Present, medium, visible in dorsal and ventral views	Present, large, visible in dorsal and ventral views	Present, small, visible in dorsal and ventral views	
Terminal caudal scale	Black	Black	Black	Black	Black	
Ventrals	225-260 (N = 21) \circlearrowleft ; 243-268 (N = 22) \circlearrowleft	210-237 (N = 35) ♂; 235-242 (N = 29) ♀	190-230 (N = 15) \circlearrowleft ; 200-238 (N = 20) \circlearrowleft	219-240 (N = 12) \circlearrowleft ; 221-258 (N = 8) \circlearrowleft	245-279 (N = 4) ♂; 268-287 (N = 4) ♀	
Subcaudals	26–36 (N = 19) \Diamond ; 24–31 (N = 19) \Diamond	26-30 (N = 34) ♂; 21-31 (N = 25) ♀	27-38 (N = 15) ♂; 24-31 (N = 20) ♀	32-36 (N = 8) \circlearrowleft ; 26-32 (N = 8) \circlearrowleft	23-30 (N = 4) \circlearrowleft ; 24-27 (N = 4) \circlearrowleft	
Supralabials	Six (rarely five or seven)	Six (rarely seven)	Six	Six	Six	
Infralabials	Six or seven	Six (rarely seven)	Seven (rarely eight)	Seven	Seven or eight	
Preocular–Nasal contact	Absent	Absent	Absent	Absent	Absent	
Tail tip shape	Slightly pointed	Slightly pointed	Pointed	Pointed	Pointed	
Hemipenes	Slightly bilobed, almost simple and noncapitate, semi- calyculate; body covered by moder- ately sized hooked spines on sulcate side	Unilobed, noncapi- tate, semicalyculate; body covered by large hooked spines on sulcate side	Unilobed, unicapi- tate, unicalyculate; body covered by moderately sized hooked spines on sulcate side	Slightly bilobed, almost simple and noncapitate, semi- calyculate; body covered by moder- ately sized hooked spines on sulcate side	-	

KOWLOSKY, 1898, Apostolepis kikoi Santos, Entiauspe-Neto, Araújo, Souza, Lema, Strüssmann & Albuquer-QUE, 2018, Apostolepis lineata COPE, 1887, Apostolepis longicaudata Gomes, 1921, Apostolepis nelsonjorgei Lema & Renner, 2004, Apostolepis niceforoi Amaral, 1935, Apostolepis nigrolineata (Peters, 1869), Apostolepis nigroterminata Boulenger, 1896, Apostolepis phillipsi Harvey, 1999, Apostolepis rondoni AMARAL, 1925, Apostolepis serrana LEMA & RENNER, 2006, Apostolepis striata LEMA, 2004, Apostolepis thalesdelemai Borges-Nojosa, Lima, Bezer-RA & JAMES, 2017, Apostolepis underwoodi LEMA & CAMP-BELL, 2017, and Apostolepis vittata (COPE, 1887) based on a combination of its uniformly red dorsal pattern with two dorsolateral black stripes (a different combination of none, three, five, seven, or eleven dorsal stripes, over red, yellow, brown, black or gray background coloration) with the presence of white and black nuchal collars (nuchal collars absent in A. ambiniger, A. breviceps, A. christineae, A. goiasensis, A. intermedia, A. lineata, A. longicaudata, A. niceforoi, A. serrana, A. striata, A. vittata, variable for A. nigrolineata and A. thalesdelemai).

Systematics: Interspecific genetic uncorrected p-distances range from 0.2–7.9% for the 16S rRNA gene fragment in *Apostolepis* species (Supplementary Fig. 2A). The p-distance between *A. quirogai* and *A. assimilis* for this gene fragment is 0.28%, suggesting a high degree of molecular similarity within the mitochondrial locus, and possibly a recent speciation event or gene flux between both species. Patristic distances inferred upon the Maximum Likelihood analysis tree range from 0.091–0.400 in *Apostolepis* species (Supplementary Fig. 2B). All sampled species of the *A. assimilis* group were recovered with low patristic distances (0.091–0.127).

Some putative synapomorphies of the *A. assimilis* group are also reinterpreted here, as inferred with our parsimonybased morphological character optimization (Supplementary Material 2–4). For instance, the A. assimilis group (C1) is supported by two ambiguous putative synapomorphies, a broad regular blotch covering all of the snout, reaching frontal and supraoculars [character state: 1(1)], and a terminal scale uniformly black on ventral surface [character state: 9(1)]. Although these characters are also supported as putative synapomorphies by Ferrarezzi et al. (2005), it should be noted that other species not assigned to the A. assimilis group also bear these characters (see Discussion). As for the clade of A. assimilis and A. quirogai (C2), we recover as unambiguous, unique, and non-homoplastic putative synapomorphies a moderately sized white nuchal collar, up to four scales wide [character state: 4(1)], a ventral scale approximate mean range of 241-261 in males, 254-280 or more in females [character state: 13(1)], and an ambiguous synapomorphy, the septomaxillary process of premaxilla short and widely separated from each other [character state: 21(0)].

As for the clade containing A. arenaria, A. cearensis, A. gaboi, and A. sanctaeritae (C₃), we recover as unambiguous, unique, and non-homoplastic the occurrence on

sandy soils [character state: 29(1)]. For unambiguous and private characters, the red or orange light snout blotch color [character state: 0(1)], present anterior indentation of black nuchal collar, on vertebral row [character state: 6(1)], narrow and subcylindrical ectopterygoid shape [character state: 24(1)], fronto-parietal suture in dorsal shape W-shaped, with an antero-medial parietal indentation between frontals [character state: 26(1)]. The sole ambiguous putative synapomorphy recovered is a large nuchal white collar, up to six scales wide [character state: 4(2)].

Geographic distribution, conservation and natural history: Apostolepis quirogai is known to occur in the Uruguayan Savanna in Misiones, northeastern Argentina, and in Rio Grande do Sul, southern Brazil (Fig. 9). It is currently recorded to seven localities and has an estimated Extent of Occurrence of 9,526.604 km² and an Area of Occupancy 28.000 km². This species is currently considered Endangered (EN) in Brazil (SALVE 2019), which is corroborated by our Extent of Occurrence and Area of Occurrence data. Despite the new records presented in this study, the range of A. quirogai has not expanded significantly, considering the new records are recovered between the easternmost (Santo Ângelo) and westernmost (Posadas) limits of the distribution for this species. The city of Posadas is located on the border between Argentina and Paraguay. It is unclear whether the Paraná river, which separates both countries, acts as a barrier for the dispersal of this species, although the lack of sampling effort in this area could explain the lack of records. We find it likely that sampling in the department of Itapuá, in Paraguay, will yield new records of this species, and its first records from this country should be expected. No detailed natural history data is available, although collection records state that specimen UFRGS 5668 was collected in a pitfall trap and specimen IBSP 93624 was encountered active at night in urban settings.

Snout osteology: Snout complex consists of premaxilla, nasals, septomaxillae, vomers, and prefrontals (Figs 10–12).

Premaxilla single, thick, robust, and edentulous, 1.6 times broader than high; posterodorsally oriented ascending process about rectangular shaped and medially notched, with small lateral wings and sharply triangular dorsal apex, slightly concave; short knob-like nasal process present, contacting anterior tips of nasals; transverse processes posterolaterally oriented, being widest part of premaxilla, and partly visible in dorsal view, distinctly separated from maxillae; posteriorly oriented vomerine processes robust, conical, slightly laterally diverging, with pointed tip, dorsally contacting anteroventral part of septomaxilla, distinctly separated from anterior end of vomers; ventral surface of premaxilla pierced by at least two foramina in anterior region, which may have smaller perforations or notches.

Nasals paired, anterior edge of dorsal lamina about half width of posterior edge, posterolateral edge strongly rounded in dorsal view; each nasal 2.3 times longer than broad (widest region); dorsal lamina convex, in medial contact along straight suture; lateral edge of dorsal lamina slightly curved downwards; posteroventral process of nasal contacts anteroventral process of frontal posteriorly but remains distinctly separated from anterior tip of parasphenoid rostrum; vertical lamina of nasals laterally contacting medial edge of septomaxillae along posterior one-fourth.

Septomaxillae paired, in dorsal view 1.9 times longer than broad (widest region), not in medial contact; each with broad ascending conchal process with blunt edges, freely extending laterally beyond lateral edge of nasal in dorsal view, but not reaching height of dorsal lamina of nasal, approaching but not contacting maxilla; anteromedial process of septomaxilla is 16% of total length of septomaxilla, curved and oriented anterolaterally, inserting between vomerine and nasal processes of premaxilla, not visible in dorsal view, with tapered edge; posteromedial process long and thin, accounts for 43% of total length of septomaxilla, laterally diverging posteriorly, contacts vertical lamina of nasal medially, rounded posterior tip contacts anteroventral tip of frontal, just lateral to ventral contact region between nasal and frontal; septomaxillary body, with complex structure partly made of only thin bone material with rounded indentation in rear view; posterior region of septomaxillary body and ventral surface of posteromedial process of septomaxilla contact anterior and dorsal region of vomer.

Vomers paired, complex structures, in dorsal view 1.4 times broader (widest region) than long, medially in contact, and with anterior and posterior regions diverging; contacting septomaxilla anteriorly and dorsally, laterally remaining slightly separated from anterior region of palatine; body of vomer made of thin bone material, globular shaped, with anteriorly oriented opening; in lateral view, slightly bifurcate vertical posteromedial laminae diverging dorsally and ventrally, framing but not contacting anterior region of choanal process of palatine.

Prefrontals paired, oriented vertically and oblique, 2.1 times higher than wide, distinctly separated from each other, forming anterior margin of orbit; in lateral view, anterior margin undulated; posterolateral margin slightly concave; anterodorsally distinctly separated from posterolateral region of nasal; dorsal edge contacts anterolateral edge of frontal along slightly oblique suture; ventral edge contacts dorsal surface of maxilla lateroventrally and maxillary process of palatine medioventrally; in rear view, large lacrimal foramen visible in ventromedial region and lacrimal process absent.

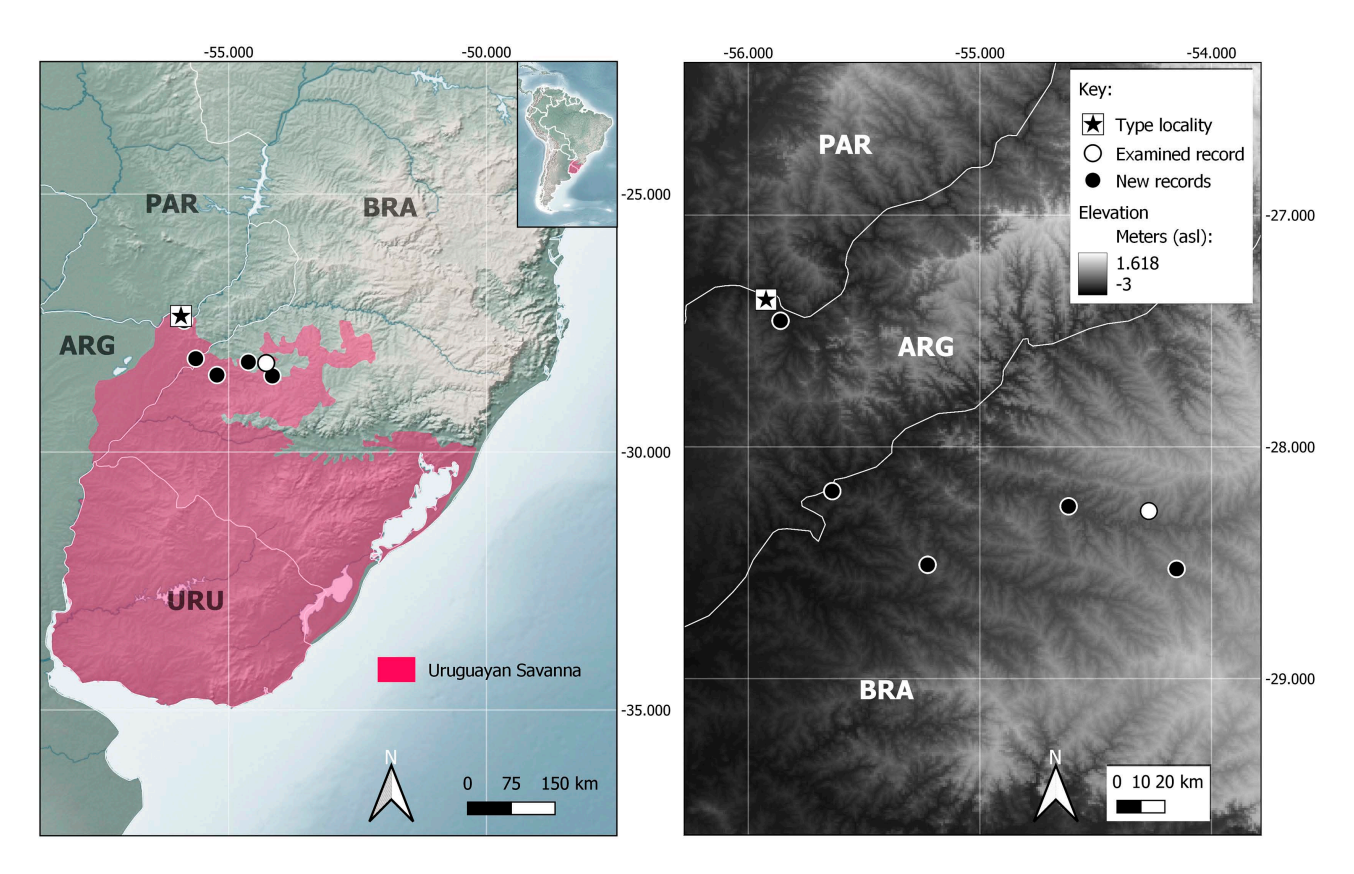


Figure 9. Geographic distribution of *Apostolepis quirogai* in South America. Left: Overview of range and distribution of *A. quirogai* within the Uruguayan Savanna (modified from Olson et al. 2001); right: overview of available records for *A. quirogai*, with type locality, examined record of Lema & Cappellari (2001), and new records. Country abbreviations: ARG = Argentina; BRA = Brazil; PAR = Paraguay.

Braincase osteology: Braincase composed of frontals, parietal, supraoccipital, prootics, exoccipitals, parabasisphenoid, and basioccipital.

Frontals paired, semicircular in dorsal view, each about twice longer than broad (widest region), dorsal lamina slightly convex, in medial contact with straight suture;

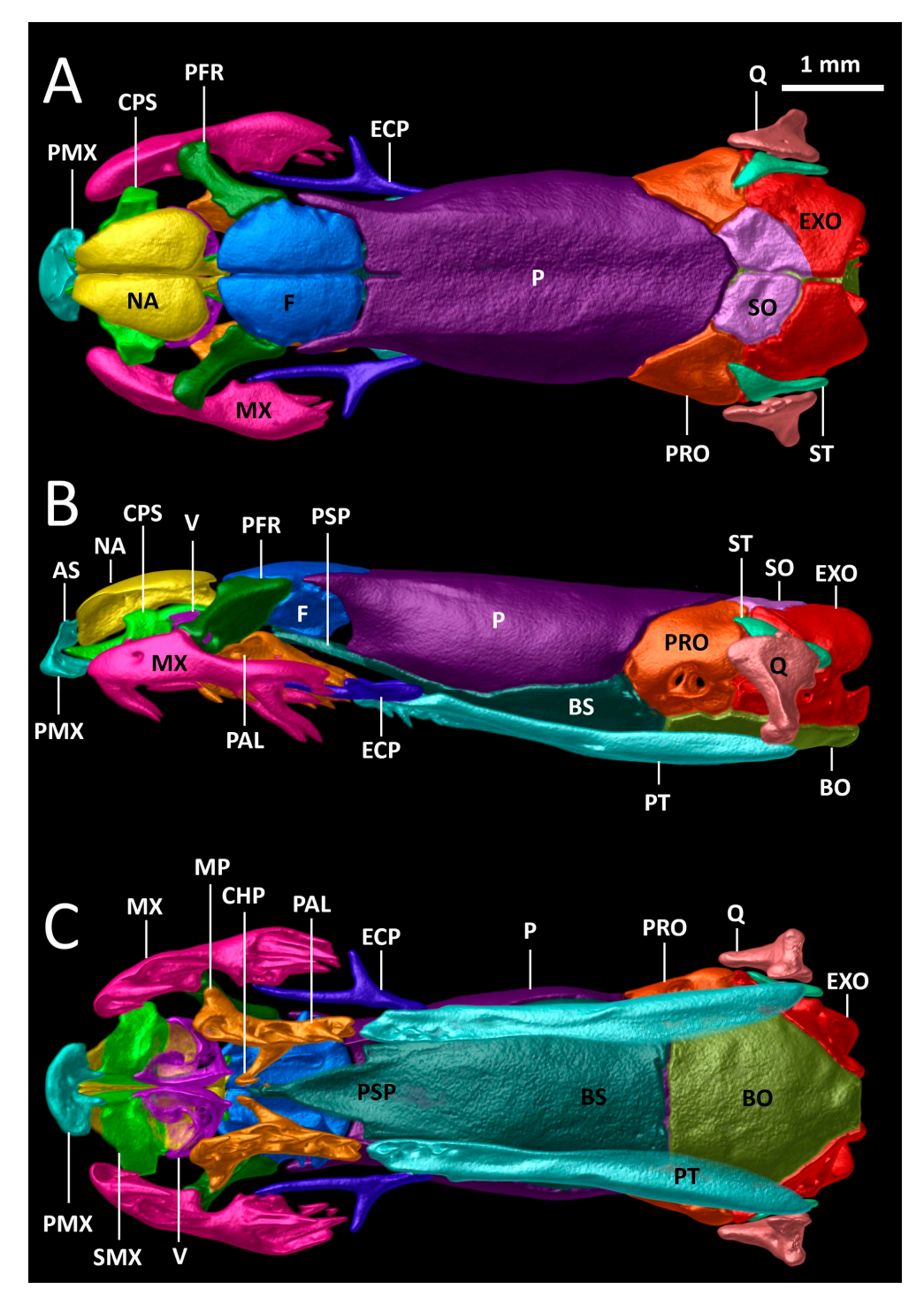


Figure 10. Micro-CT images of the skull without mandibles of *Apostolepis quirogai* (UFRGS 6676) in (A) dorsal, (B) lateral, and (C) ventral views; AS (ascending process of premaxilla); BO (basioccipital); BS (basisphenoid); CPS (conchal process of septomaxilla); ECP (ectopterygoid); EXO (exoccipital); F (frontal); MP (maxillary process of palatine); MX (maxilla); NA (nasal); P (parietal); PAL (palatine); PFR (prefrontal); PMX (premaxilla); PRO (prootic); PSP (parasphenoid rostrum); PT (pterygoid); Q (quadrate); SMX (septomaxilla); SO (supraoccipital); ST (supratemporal); V (vomer). Scale bar = 1 mm.

Table 3. In this section, we compare the skull of *A. quirogai* to that of skulls of *A. ambiniger, A. albicollaris, A. assimilis, A. cearensis,* and *A. sanctaeritae* described by Ferrarezzi et al. (2005) and Entiauspe-Neto et al. (2020, 2021a, 2021b, 2022). Characters are as follows: C.1 = Lateral wings on ascending process of premaxilla; C.2 = posterior processes of the premaxilla; C.3 = frontal edge of nasals; C.4 = nasal to prefrontal contact; C.5 = ventral edge of prefrontal contacts maxillary process of palatine; C.6 = frontal shape; C.7 = shape of posterior border of parietal; C.8 = tooth-like spur at posterior end of maxillae; C.9 = maxilla and medial process of ectopterygoid contact; C.10 = vomer to palatine contact; C.11 = parietal to parasphenoid rostrum contact; C.12 = supraoccipital condition; C.13 = prearticular crest of compound bone; C.14 = number of dentary teeth; C.15 = number of pterygoid teeth; C.16 = shape fronto-parietal suture in dorsal view; C.17 = number of anterior maxillary teeth; C.18 = number of palatine teeth. Data was obtained from Entiauspe-Neto et al. (2021), (2020²), (2021a³-b⁴), Ferrarezzi et al. (2005⁵), and this study ⁶. Species groups: DIM = *A. dimidiata* species group; ASI = *A. assimilis* species group.

	A. albicollaris ¹	A. ambiniger ²	A. sanctaeritae³	A. cearensis ⁵	A. assimilis ⁴	A. quirogai ⁶
Species group	DIM	DIM	ASI	ASI	ASI	ASI
C.1	Large	Large	Medium	?	Medium	Small
C.2	Blunt	Blunt	Pointed	?	Pointed	Pointed
C.3	V-shaped	V-shaped	V-shaped	V-shaped	V-shaped	Straight
C.4	Present	Present	Absent	Present	Absent	Present
C.5	Present	Absent	Present	?	Present	Present
C.6	Semicircular	Rectangular	Semicircular	Semicircular	Semicircular	Semicircular
C.7	Straight	Straight	Slightly wavy	Straight	Wavy	Curved
C.8	Present	Absent	Present	?	Absent	Absent
C.9	Present	Absent	Absent	?	Absent	Present
C.10	Present	Absent	Absent	?	Absent	Absent
C.11	Present	Present	Present	?	Present	Absent
C.12	Single	Single	Single	Single	Single	Paired
C.13	Higher than surangular crest	As low as surangular crest	Higher than surangular crest	As low as surangular crest	Higher than surangular crest	Lower than surangular crest
C.14	6	5-6	8–9	7–8	7–8	8-9
C.15	0-1	0	4-5	2	4	4
C.16	U-Shaped	U-Shaped	U-Shaped	W-Shaped	U-Shaped	U-Shaped
C.17	4	4	4	4	4	3
C.18	3–5	4	5	5	5	4-5

small portion directly behind region of greatest width of frontal participates in formation of dorsal margin of orbit; anterolateral edge forming oblique, curved suture with prefrontal; loose, curved suture between frontals and parietal, with long anterolateral processes of parietal extending along lateral edges of frontals and almost reaching contact zone with prefrontals, excluding major parts of frontals from orbit; frontal contacts nasal anteroventrally and lateral to this contact zone, a process contacts posterior end of posteromedial process of septomaxilla with its anterior surface; laterally each frontal has ventromedially oriented concave lamina, that contacts its counterpart medially along anterior fourth of its length; anteromedially, frontal exhibits vertical lamina that is fused ventrally with lateral lamina to form a short tubular structure in anterior region of each frontal, with vertical laminae of both frontals in firm medial contact; posterior to tubular structure, lateral lamina of both frontals clearly separated, with their medial margins approximately parallel to each other; only end of tip of parasphenoid rostrum contacts posterior margin of contact zone of vertical laminae of frontals.

Parietal single, elongate, 1.7 times longer than wide, roughly ellipsoid in dorsal view except for anterolateral processes; dorsal surface slightly convex, except for an in-

conspicuous depression, longitudinally along its midline; anteriorly, is a short medial groove, about 10% of length of median region; anterolateral processes moderately long and thin, framing posterolateral half of each frontal and forming posterodorsal margins of orbits; anterior border (ignoring anterolateral processes) slightly concave, and posterior border strongly convex curved; anterolateral processes diverge slightly laterally anteriorly; weakly pronounced ridge extends dorsally on both sides from anterolateral process in posterior direction, almost reaching suture with supraoccipital, both ridges slightly approach each other posteriorly, but remain distinctly separated from each other; lateral to dorsal ridges, parietal slopes downwards with a convex surface to meet ventrally most of basisphenoid portion of parabasisphenoid but without contacting parasphenoid rostrum; posterolaterally parietal contacts dorsal and anterior margins of prootics and forms anterior limit of foramen for maxillary branch of trigeminal nerve at lateral suture with prootic; oblique, V-shaped posterodorsal sutures with supraoccipital. Postorbitals absent.

Supraoccipital apparently broken into two pieces, giving a paired appearance, each piece about diamond-shaped and as broad as long, with almost straight anterior and posterior borders, in medial contact with an almost straight

suture; right part of supraoccipital partly fused with right exoccipital in posterior region; supraoccipital contacts parietal anteriorly, prootics anterolaterally, exoccipitals posteriorly, and remains distinctly separated from supratemporals; laterally supraoccipital extends downwards (internal) to contribute to dorsomedial walls of otic capsules.

Paired prootics ovaloid in lateral view, 1.1 times higher than long; each prootic contacts parietal anteriorly and anterodorsally, supraoccipital posterodorsally, exoccipital posteriorly, parabasisphenoid complex anteroventrally, basioccipital posteroventrally, and anterior part of supratemporal laterally, but remains slightly separated from quad-

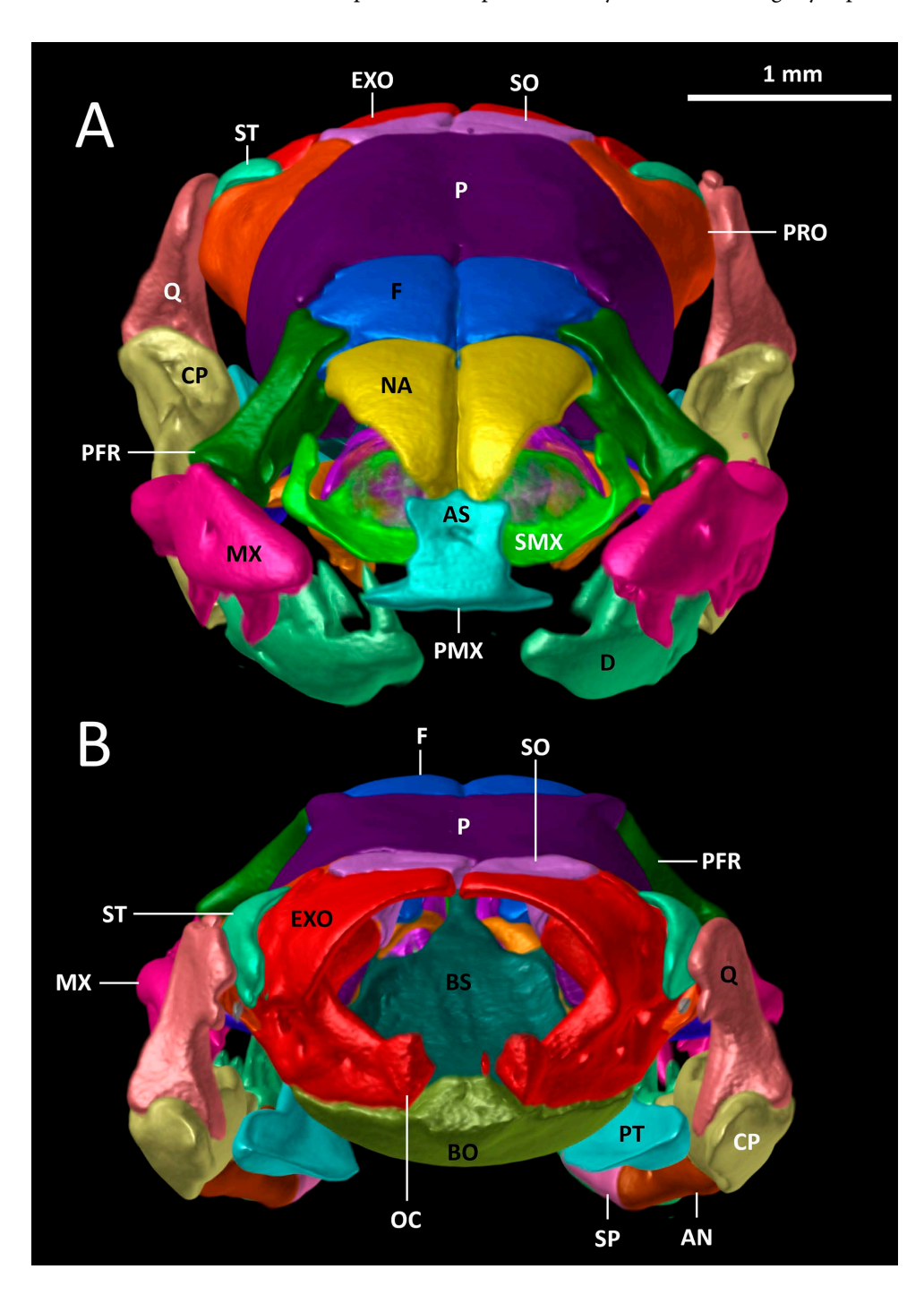


Figure 11. Micro-CT images of the skull of *Apostolepis quirogai* (UFRGS 6676) in (A) anterior and (B) posterior views; AN (angular); AS (ascending process of premaxilla); BO (basioccipital); CP (compound bone); D (dentary); EXO (exoccipital); F (frontal); MX (maxilla); NA (nasal); OC (occipital condyle); P (parietal); PFR (prefrontal); (premaxilla); PRO (prootic); PT (pterygoid); Q (quadrate); SMX (septomaxilla); SO (supraoccipital); ST (supratemporal). Scale bar = 1 mm.

rate; at suture with parietal, prootic forms posterior border of foramen for maxillary branch of trigeminal nerve; at suture with exoccipital, prootic forms anterior margin of fenestra ovalis; three other foramina on lateral surface of prootic: small foramen for dorsal constrictor branch of trigeminal nerve situated in anteroventral region close to suture with parabasisphenoid complex, and two medium-sized foramina slightly posterior and slightly ventral to medial region of prootic; in dorsal view, prootic bears conspicuous depression in posterior region, in which anterior tip of supratemporal rests; prootic contributes to formation of anteroventral, anteromedial and anterolateral wall of otic capsule; few small foramina pierce medial laminae of each prootic.

Columella hardly visible in CT scan data.

Paired exoccipitals irregularly shaped, and slightly separated from each other by straight medial suture; each with oblique, dorsolateral ridge parallel to inner margin of re-

spective supratemporal; each exoccipital contacts supraoccipital anterodorsally, prootic anterolaterally, basioccipital ventrally, and supratemporal dorsolaterally; fenestra ovalis situated at suture between prootic and exoccipital, and exoccipital forms posterior margin of fenestra; four small foramina pierce lateral wall of each exoccipital; exoccipital contributes to formation of posteroventral, posteromedial and posterolateral wall of otic capsule; exoccipital is most posteriorly projecting bone of skull roof and posteriorly forms dorsal, lateral, and lateroventral border of foramen magnum, with exoccipital components of occipital condyle remaining distinctly separated, and thus not excluding posterior process of basioccipital from participation in foramen magnum.

Single basioccipital ovaloid, 1.1 times longer than broad, with convex ventral lamina; contacts parabasisphenoid complex anteriorly, prootics anterolaterally, and exoccipitals posterolaterally; posterodorsally basioccipital is partic-

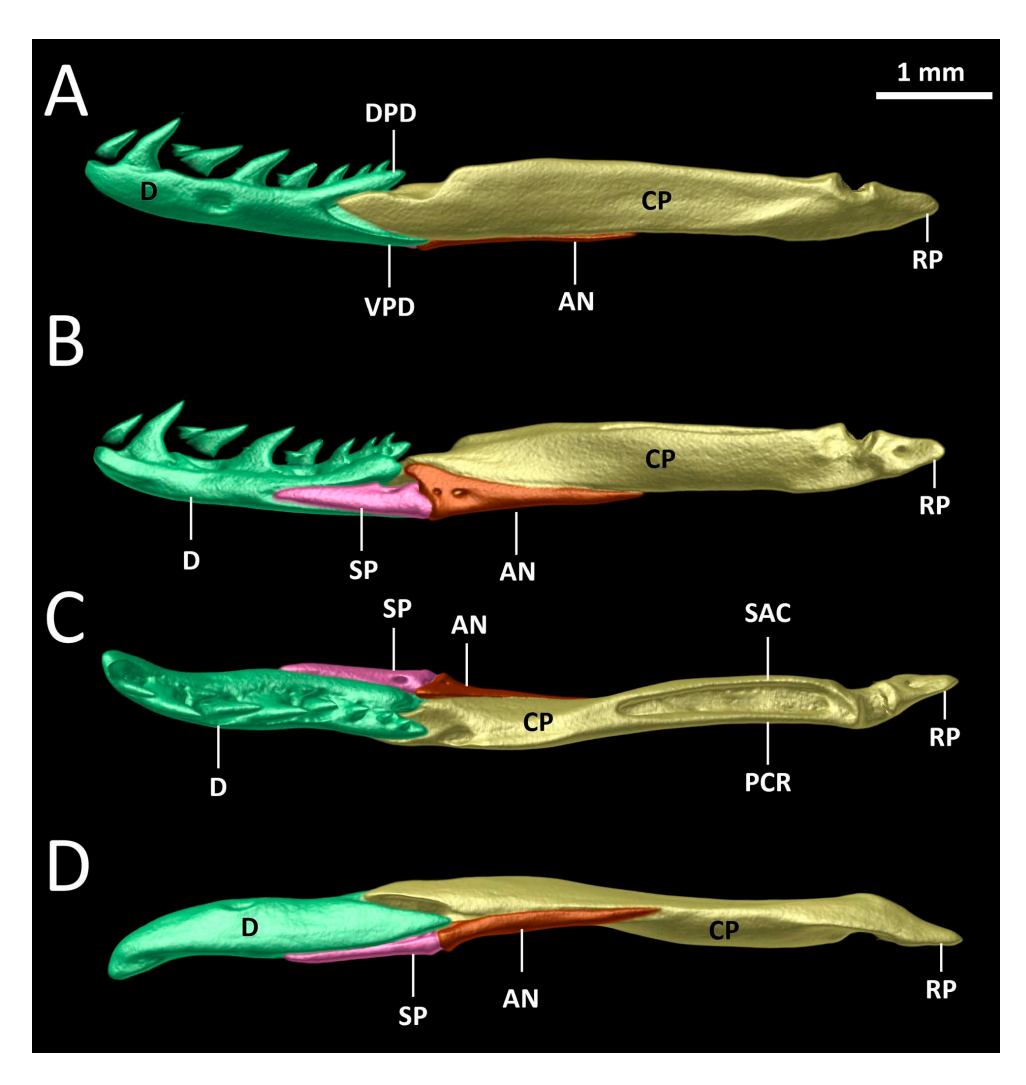


Figure 12. Micro-CT images of the left mandibula of *Apostolepis quirogai* (UFRGS 6676) in (A) lateral, (B) lingual, (C) dorsal, and (D) ventral views; AN (angular); CP (compound bone); D (dentary); DPD (dorsal process of dentary); PCR (prearticular crest of compound bone); RP (retroarticular process of compound bone); SAC (surangular crest of compound bone); SP (splenial); VPD (ventral process of dentary). Scale bar = 1 mm.

ipating in formation of foramen magnum; posterior end of basioccipital (part of occipital condyle), straight in transverse direction in ventral view and trapezoidal in posterior view; widest part of basioccipital distinctly posterior to sutures with prootics and exoccipitals; surface of basioccipital relatively smooth and lateral edges almost straight, without backwards pointing projections.

Unpaired parasphenoid and basisphenoid fused to form parabasisphenoid complex, forming an elongate structure, approximately 2.2 times longer than broad (widest region), that occupies most of skull floor, being concave in parasphenoid region and convex in basisphenoid region; basisphenoid portion roughly square shaped, and parasphenoid rostrum lanceolate with pointed anterior tip; anterior tip of parasphenoid rostrum contacts frontals ventromedially; anterior tip of parasphenoid rostrum does not surpasses anterior border of frontals in ventral view; after about first quarter, parasphenoid rostrum widens abruptly and there is an anterior Vidian foramen on each side of widened area, its opening visible in anterior view; parasphenoid rostrum distinctly separated from posteroventral region of nasals, choanal processes of palatines, posterior ending of vomers, and septomaxillae; dorsolaterally parabasisphenoid contacts parietal, and prootics posterior to it, reaching its greatest width at sutures between parietal and prootics; two posterior Vidian foramina located on each side in posterolateral part of basisphenoid portion, near suture with prootics; posterior suture with basioccipital almost straight in transverse direction.

Palatomaxillary arch osteology: Palatomaxillary arch composed of maxillae, ectopterygoids, palatines, and pterygoids.

Maxillae elongate, account for about 29% of skull length, and about 4.7 times longer than high (ignoring teeth), extending from level of anterior margin of nasals to posterior region of orbit, forming most of lower margin of orbit laterally; highest point (ignoring teeth) located at anterior contact point with prefrontal; maxillae slightly arched towards premaxilla; ventral surface of maxilla bears three anterior tooth loci, with curved, and rear facing teeth, followed posteriorly, after small diastema, by pair of large grooved fangs, situated below eye; posterior end of maxilla slightly bifurcate but without tooth-like spur at lateral margin of ventral surface; maxilla contacts prefrontal on its dorsal surface and contacts medial process of ectopterygoid medially; palatine process short and rounded, located behind anterior tooth line, approaches but not contacts maxillary process of palatine; ectopterygoid process not evident.

Paired ectopterygoids deeply bifurcated anteriorly, giving it a Y-shape, with medial process about 2.9 times longer than lateral process; in dorsal view of skull, ectopterygoids almost completely visible and only posterior edge overlapped by braincase; medial and lateral processes located anteriorly, directed anterolaterally and frame posterior end of maxilla laterally and medially; medial process contacts maxilla medially but lateral process remains separated from it, forming an open maxillo-ectopterygoid fenestra; ventrolateral surface of flattened posterior process has

small facet, where it contacts dorsal surface of anterolateral portion of pterygoid.

Paired pterygoids flattened, elongated and slender, approximately 9.7 times longer than broad, corresponding to slightly more than half of skull length; not visible in dorsal view of skull, covered by parietal and prootics; ventral surface bears four tooth loci; teeth subequal, smaller than maxillary teeth, slightly curved, rear facing; anteromedial tip of pterygoid approaches, but not does not contact or reach level of palatine; medial border slightly convex, lateral border almost straight; smallest distance between both pterygoids located shortly after tooth line; greatest distance between both pterygoids located at their posterior tips; not in contact with other skull bones except for ectopterygoid; in dorsal view surface of pterygoid concave; posterior end of pterygoid terminates clearly before level of posterior end of basioccipital.

Palatines elongated, approximately 5.8 times longer than broad, excluding choanal and maxillary processes, corresponding to 20% of skull length, and represent shortest of all toothed bones; medial edge convexly curved; ventral surface bears four (left palatine) or five (right palatine) tooth loci; teeth solid, subequal, curved, and rear facing; palatine only contacts medioventral region of prefrontal through dorsal surface of its maxillary process and dorsal lamina of anterior end of palatine very close to posterior wing of vomer, but without touching it; dorsomedially, long, medium-sized choanal process rises and curves downwards in semicircle, with broad base and sharp tip, approaching but remaining distinctly separated from its counterpart medially; maxillary process thumb-like, situated on lateral surface of palatine at level of first and second tooth, directed anterolaterally, approaching but not contacting palatine process of maxilla; posterior part of palatine behind tooth line bifurcated into ventrolateral and dorsomedial process of subequal length, both tapering towards posterior end.

Suspensorium and mandible osteology: Suspensorium composed of supratemporals and quadrates. Each mandible composed of dentary, splenial, angular, and compound bone.

Paired supratemporals laminar, elongated, about 2.8 times longer than wide; in dorsal view, about triangular or boomerang-shaped, with lateral edge forming almost right angle; in dorsal view, each supratemporal overlaps and firmly contacts small region in posterior part of prootic, and anterolateral part of exoccipital over well-defined facets; it approaches dorsomedial region of quadrate, but remains marginally separated from it; posterior tip of supratemporal freely extends and protrudes posteriorly beyond quadrate (not being in contact with other skull bones) but terminates distinctly before posterior end of exoccipital; posterior tips slightly approaching each other.

Paired quadrates flattened and broad dorsally, tapering dorsoventrally in lateral view, with lateral lamina twisted along its axis, gradually increasing in width in ventral direction in rear view; slightly oriented obliquely, from anterodorsally to posteroventrally; posterodorsal part approaches mediolateral region of supratemporal to only marginal distance; medial part has short process, which corresponds to contact region with columella auris; ventral part bifurcated, with medial branch being broader and longer than lateral branch and both together spanning glenoid cavity of retroarticular process of mandible; quadrate not exceeding posterior limit of skull roof.

Paired dentaries elongate and slender, slightly curved anteromedially, about 8.1 times longer than high, making up approximately 42% of mandible length; dorsal surface bears eight (left dentary) or nine (right dentary) tooth loci; teeth subequal, curved and rear facing; lateral face slightly convex with mental foramen located at about level between third and fourth (left dentary) or below fifth (right dentary) tooth, in medial region of dentary; at about level of sixth (right dentary) or seventh (left dentary) tooth, dentary branches into shorter dorsal process, which overlays anterior part of compound bone, and longer lanceolate ventral process; gap between dorsal and ventral processes mainly filled by splenial medially and by anterior portion of compound bone laterally, whereas posteriormost part of ventral process contacts anteroventral part of angular; ventral process runs with its dorsal surface parallel and close along anterior part of medioventral region of compound bone without touching it; in medial view, dorsal process bifurcated in its posterior region, at level of last or penultimate tooth, with slightly longer tooth-bearing dorsolateral branch and edentulous ventromedial branch.

Splenials elongate, triangular, tapered anteriorly, about 4.4 times longer than high, smallest of mandibular bones, making up about 18% of mandibular length; anterior mylohyoid foramen positioned dorsal to midline in posterior part of bone; posterior edge of splenial firmly contacts anterior region of angular along oblique suture.

Angulars elongate, triangular, tapered posteriorly, almost four times longer than high, and represent second smallest of mandibular bones, making up about 28% of mandibular length; each angular contacts splenial anteriorly, compound bone laterally and dorsally, and posteromedial surface of tip of ventral process of dentary; posterior mylohyoid foramen centrally positioned in anterior third of bone; small foramen pierces dorsolateral anterior surface of angular, anterior to posterior mylohyoid foramen and shortly posterior to suture with splenial.

Compound bones elongate and slender, about eight times longer than high, and represent largest of mandibular bones, making up about 70% of mandible length; surangular crest covers almost half of bone, slightly higher than prearticular crest and thus prearticular crest not visible in lateral view; in lateral view, compound bone tapers anteriorly, fitting between dorsal and ventral processes of dentary, dorsally contacting ventral surface of dorsolateral process, but not contacting ventral process; anterodorsally oriented foramen present in anterior region on dorsal surface of compound bone; retroarticular process long, slightly medially directed, and reaching level of posterior end of exoccipital.

Comparative osteology of Apostolepis: In this section, we compare the skull of A. quirogai to that of skulls of A. ambiniger, A. albicollaris, A. assimilis, A. cearensis, and A. sanctaeritae described by Ferrarezzi et al. (2005) and Entiauspe-Neto et al. (2020, 2021a, 2021b, 2022). Certain characters of the skull of A. quirogai differ among species of Apostolepis (characters in parentheses): small lateral wings on ascending process of premaxilla (vs. broad lateral wings in A. albicollaris); sharply triangular dorsal apex of ascending process of premaxilla (vs. stout in A. ambiniger, A. assimilis and A. sanctaeritae); transverse processes define widest part of premaxilla (vs. lower region of ascending process defines widest part of premaxilla in A. ambiniger); transverse processes of premaxilla are partly visible in dorsal view (vs. not visible in A. ambiniger); pointed posterior processes of premaxilla (vs. blunt in *A. albicollaris* and A. ambiniger); front edges of nasals not forming a V-shape (vs. front edges forming a broad V-shape that contacts and frames ascending process of premaxilla in A. albicollaris, A. ambiniger, A. assimilis, A. cearensis, and A. sanctaeritae); nasal and prefrontal not in contact (vs. in contact in A. albicollaris, A. ambiniger, and A. cearensis); dorsal laminae of nasals and frontals not in contact (vs. in contact in A. albicollaris and A. ambiniger); vertical lamina of nasals laterally contacting medial edge of septomaxillae (vs. not contacting medial part of septomaxillae in A. sanctaeritae); nasals remain distinctly separated from parasphenoid rostrum (vs. posteroventral tip of nasal contacts anterior tip of dorsally oriented process of parasphenoid rostrum in A. albicollaris and A. ambiniger); anterior tip of parasphenoid rostrum does not surpasses anterior border of frontals in ventral view (vs. surpasses anterior border of frontals in A. ambiniger); ascending conchal process of septomaxilla freely extending laterally beyond lateral edge of nasal and largely visible in dorsal view (vs. marginally visible in A. ambiniger); vomers medially in contact (vs. not contacting each other medially in A. ambiniger and A. assimilis); vomers not in contact with palatines (vs. vomers laterally contacting anterior region of palatines in A. albicollaris); prefrontals are about 2.1 times higher than broad (vs. 1.5 times higher than broad in A. ambiniger); ventral edge of prefrontal contacts maxillary process of palatine (vs. not in contact in A. ambiniger); each frontal is semicircular in dorsal view (vs. rectangular in A. ambiniger); Ushaped fronto-parietal suture in dorsal view without parietal indentation between frontals (vs. W-shaped suture, with an antero-median parietal indentation in A. cearensis); parietal roughly ellipsoid in dorsal view (vs. roughly rectangular in A. albicollaris, A. ambiniger, and A. albicollaris); anterior border of parietal is almost straight in transverse direction (vs. anterior border is strongly concave in A. albicollaris, A. assimilis, and A. sanctaeritae); posterior border of parietal is strongly convex curved (vs. posterior border is almost straight in transverse direction in A. albicollaris, A. ambiniger, and A. sanctaeritae); weakly pronounced parietal ridges (vs. well-pronounced in A. assimi*lis*); parietal ridges slightly approach each other posteriorly (vs. both ridges are about parallel to each other in A. ambiniger; vs. both ridges merge in posterior fifth of parietal, and reach to suture with supraoccipital in *A. sanctaeritae*); parietal does not contact parasphenoid rostrum (vs. contacts posterior half of parasphenoid rostrum in A. albicollaris, A. assimilis and A. sanctaeritae); exoccipital components of occipital condyle approaching but remaining distinctly separated from each other, so that posterior process of basioccipital is not excluded from participation in foramen magnum (vs. exoccipital components of occipital condyle are in close contact, excluding posterior process of basioccipital from participation in foramen magnum in A. ambiniger); exoccipital is most posteriorly projecting bone of skull roof (vs. supratemporal is most posteriorly protruding bone of skull roof in A. assimilis); parabasisphenoid and basioccipital bones not fused (vs. fused in A. assimilis); parabasisphenoid concave in parasphenoid region (vs. straight in A. assimilis); widest part of basioccipital is distinctly posterior to sutures with prootics and exoccipitals (vs. widest part is at suture with prootics and exoccipitals in A. ambiniger); surface of basioccipital is relatively smooth (vs. slightly elevated in anterior region in A. albicollaris; vs. in anterior third is a slight elevation medially which ends posteriorly in two symmetrical bulges, each lateral to midline in A. sanctaeritae); lateral edges of basioccipital are almost straight, without backwards pointing projections (vs. approximately at beginning of posterior half of basioccipital, is a short, blunt, backwards pointing projection on each side of outer lateral edges in A. sanctaeritae and A. assimilis); posterior end of basioccipital (part of occipital condyle) is trapezoidal in posterior view (vs. quadrant-shaped in A. ambiniger); ventral surface of maxilla bears three anterior tooth loci (vs. 4 anterior tooth loci in A. albicollaris, A. ambiniger, A. assimilis, and A. sanctaeritae); posterior end of maxilla without a toothlike spur at lateral margin of ventral surface (vs. presence of a tooth-like spur at lateral margin of ventral surface in A. albicollaris and A. sanctaeritae); maxillae extend to posterior region of orbit (vs. extend to about central region of orbit in A. assimilis and A. sanctaeritae); maxilla contacts medial process of ectopterygoid medially (vs. not in contact in A. ambiniger, A. assimilis, and A. sanctaeritae); medial process of ectopterygoid about 2.9 times longer than lateral process (vs. medial process 1.4-1.9 longer than lateral process in A. albicollaris; vs. medial process slightly longer than lateral process in A. assimilis and A. sanctaeritae); 4 pterygoid tooth loci (vs. o-1 in A. albicollaris; vs. edentulous in A. ambiniger; vs. 2 in A. cearensis); pterygoids are approximately 9.7 times longer than broad (vs. 6.5 times longer than broad in A. assimilis); lateral border of pterygoids is almost straight (vs. slightly curves posterolaterally in A. albicollaris and A. assimilis); pterygoids are not visible in dorsal view of skull (vs. lateral edges are visible and not covered by any bone in A. sanctaeritae); anteromedial tip of pterygoid does not reach level of palatine (vs. anteromedial tip of pterygoid dorsally overlaps marginally posteromedial tip of palatine without touching it in A. ambiniger and A. sanctaeritae); posterior ends of pterygoids terminate clearly before level of posterior end of basioc-

cipital (vs. reach posterior end of basioccipital in A. assimilis); palatines are approximately 5.8 times longer than broad (vs. 7.3 times longer than broad in A. ambiniger); medial edge of palatines is convexly curved (vs. straight in A. ambiniger); lateral edges of supratemporals are almost right-angled in dorsal view (vs. slightly curved in A. albicollaris, A. ambiniger, and A. sanctaeritae; vs. almost straight and twisted in posterior half in A. assimilis); supratemporal overlaps and firmly contacts a small region in posterior part of prootic (vs. more than posterior half of prootic in A. albicollaris; vs. posterior half of prootic in A. ambiniger and A. sanctaeritae); posterior tip of supratemporal terminates distinctly before posterior end of exoccipital (vs. terminates slightly before posterior end of exoccipital in A. albicollaris; vs. protrudes posterior end of exoccipital in A. assimilis); dentary with 8-9 tooth loci (vs. 6 in *A. albicollaris*; vs. 5–6 in *A. ambiniger*); in medial view, dorsal process of dentary is bifurcated in its posterior region, at level of last or penultimate tooth, with a slightly longer tooth-bearing dorsolateral branch and an edentulous ventromedial branch (vs. dorsal process slightly bifurcated in its posteriormost region, distinctly behind last tooth in A. albicollaris and A. ambiniger); surangular crest of compound bone is slightly higher than prearticular crest and thus prearticular crest is not visible in lateral view (vs. prearticular crest is slightly higher than surangular crest and thus (marginally) visible in lateral view in A. albicollaris, A. assimilis, and A. sanctaeritae; vs. prearticular and surangular crests are about similar in height in A. ambiniger and A. cearensis); retroarticular process is long (vs. short in *A. sanctaeritae*).

Discussion

Our rediscovery provides the first known records of *Apostolepis quirogai* after 22 years, and raises the number of known localities from two to seven. These localities are relatively close to one another and located between previously known limits of its geographic distribution in Misiones province and Rio Grande do Sul state. *Apostolepis quirogai* remains a range-restricted species, known solely from a small portion of grassland areas in southern Brazil and northeastern Argentina. Although suitable grassland habitat exists in the southernmost portion of the Uruguayan Savannas, ranging from central Rio Grande do Sul southwards into Uruguay and Argentina, it is unlikely that *A. quirogai* occurs in this area, considering that the region has been extensively sampled (see Alvares et al. 2022).

Our phylogenetic hypothesis over molecular data unambiguously suggests the inclusion of *A. quirogai* in the *A. assimilis* group, with high support (bootstrap < 90), as well as the congruent analyses of uncorrected p-distances and patristic distances. Previous disagreements in systematic relationships of these species, such as the inclusion of *A. quirogai* in the *A. dimidiata* species group by Lema (2001) and Lema et al. (2004), which was later contested by Ferrarezzi et al. (2005), are associated with the use of

variable morphological characters as putative synapomorphies. Sampled terminals from the *A. dimidiata* species group were recovered as monophyletic. Another Elapomorphini species group, the *Phalotris tricolor* group, is recovered as polyphyletic in our ML analysis, with *P. mertensi* nested as a sister-species to the *P. nasutus* group. A revised taxonomic arrangement for *Phalotris* transcends the scope of this work, and we highlight the need for thorough analysis in the *P. tricolor* species group.

Although preliminary, we provide the first comprehensive osteological comparison for *Apostolepis*, which sheds light into the diversity of morphological features presented by species of this genus and possible diagnostic features of osteological characters. Some characters appear to be widely conserved, such as the frontal shape, which is semicircular in all sampled *Apostolepis* species other than *A. ambiniger*, and the supraoccipital condition, being single in all species except for *A. quirogai*. Other structural

osteological characters, such as the shape of the posterior border of the parietal may be exceedingly variable, with most species bearing different shapes. Notably, species of the A. dimidiata species group are shown to have fewer pterygoid teeth (o-1) than species of the A. assimilis species group (2-5). Another character, the number of dentary teeth, also appears to be reduced in species from the A. dimidiata species group (5-6), while species of the A. assimilis group attain higher counts (7-9). Species of the A. dimidiata group also have comparatively larger lateral wings on ascending process of premaxilla than its counterparts from the A. assimilis group. The paired supraoccipital of A. quirogai could represent an artifact of preparation or an individual condition, such as a broken bone; however, it cannot be ruled out that this may constitute a unique character among congeners. It should be noted that these osteological descriptions are based on limited series, and still need to be tested for their variation and polymorphism,

Autapomorphies Outgroup A. assimilis A. quirogai A. sanctaeritae A. cearensis 2 2 Character key Unambiguous, unique, A. arenaria non-homoplastic Unambiguous, private Unambiguous, non-private A. gaboi **Ambiguous**

Figure 13. Parsimony-based morphological character optimization of the *Apostolepis assimilis* species group inferred with YBYRÁ, modified from matrix of Ferrarezzi et al. (2005), over molecular inferences of Maximum Likelihood. Nodes are labeled with unambiguously optimized morphological synapomorphic characters (black square = unique, non-homoplastic; red square = non-unique, homoplastic; blue square = unique, homoplastic; character number = value below or above squares; derived character-states = value inside squares). Gray branches represent two missing species tentatively included in the *A. assimilis* species group based on morphology. Major supported clades are outlined (C1: *A. assimilis* species group; C2: *A. assimilis* and *A. quirogai*; C3: *A. arenaria*, *A. cearensis*, *A. gaboi*, and *A. sanctaeritae*).

which are known to be prevalent in snakes (Arnold 1993, Andjelković et al. 2016). Nonetheless, the varying degrees of success in analytical classification and distinction of specimens using external morphology in our PCA, PLSDA, and DFA analyses highlight the need for integrative taxonomy tools, such as molecular systematics and microCT based osteological data, which should assist in obtaining valuable data for the identification of specimens.

We recover characters 1(1), a broad regular blotch covering all of the snout, reaching frontal and supraoculars, and 9(1), a terminal scale uniformly black on ventral surface, as putative morphological synapomorphies of the A. assimilis group, in agreement with FERRAREZZI et al. (2005), although these results should be seen as provisional (Fig. 13). For instance, the taxa A. niceforoi, A. rondoni, and A. tenuis are known to have a broad regular cream blotch covering all of the snout, and the enigmatic species Parapostolepis polylepis also bears a terminal scale uniformly black on ventral surface. These species were formerly assigned to other species groups or genus by previous authors, and have not been included in any formal phylogenetic analysis. Therefore, we find it likely that including other congeners in the molecular or morphological phylogenetic hypothesis of *Apostolepis* might lead to changes in the content of the A. assimilis and other species groups. The taxonomic status of A. arenaria and A. gaboi, its morphological variation, and phylogenetic relationships with congeners of the A. assimilis group, also needs to be formally evaluated, as no available tissue sample or osteological description are available to these species. Nonetheless, the inclusion of A. arenaria and A. gaboi within a clade with A. cearensis and A. sanctaeritae remains supported by at least six characters (Clade C₃). Furthermore, while A. assimilis, A. cearensis, A. sanctaeritae and A. quirogai share pointed posterior processes of the premaxilla, the lack of available osteological data for other species precludes us from assuming this character as a morphological synapomorphy. We believe that taxonomic arrangements made based upon small samples or incomprehensive geographic sampling have contributed negatively to the present taxonomic instability of elapomorphine snakes, and therefore, we urge authors to avoid these practices. These, and other questions, remain to be addressed by further studies on elapomorphine snakes, pending upon the availability of a higher sample of voucher specimens for external morphological analyses, for osteological analyses, and tissue samples to be sequenced for phylogenetic analyses.

Acknowledgements

This work is dedicated to H. Ferrarezzi (IBSP), for his lifelong contribution to the systematics of Elapomorphini. We thank A. Lopez (INML), L. J. Vitt (OK), M. Duarte and A. D. Abegg (IBSP), C. S. Bernardes, and P. Martins for kindly providing photographs of specimens in life. The curators and staff A. Argôlo (UESC), A. L. Prudente (MPEG), A. Kluge and D. Rabosky (UMMZ), C. J. Franklin, E. N. Smith, and J. Campbell (UTA), D. Loebmann (FURG), D.M. Borges-Nojosa (CHUFC),

D. KLINGBERG JOHANSSON and P. R. MØLLER (ZMUC), D. ME-NEGHELLI (UFRO-H), D. SANTANA (ZUFMS), E. M. X. FREIRE (MUFAL), E. LANGAN and A. WYNN (USNM), C. STRÜSSMANN (UFMT-R), F. G. GRAZZIOTIN, L. M. CORRÊA, V. J. GERMANO, and G. PUORTO (IBSP), G. SKUK (in memoriam, MUFAL), G. Colli (CHUNB), G. Cotta (FUNED), G. Köhler (SMF), H. ZAHER (MZUSP), L. GONZALES and S. REICHLE (MNKR), L. VOHNNAHME, D. KIZIRIAN, D. GARCÍA-COBOS, and L. P. NUÑEZ (AMNH), F. WERNECK (INPAH), J. MATA (FMNH), J. MARTÍN-EZ (MCZ), J. C. MOURA-LEITE (MHNCI), M. CALDERÓN and G. M. Fabián-Rangel (ICN), M. Moura (MZUFV), M.-O. Röd-DEL (ZMB), N. GILMORE (ANSP), N. VIDAL (MNHN), N. CAMA-CHO (LACM), P. CACCIALI and H. CABRAL (MHNP), P. MANZANI (ZUEC), P. CAMPBELL (BMNH), R. LIRA-DA-SILVA (MZUFBA), R. Brown (KU), and S. Schweiger (NMW), kindly loaned specimens under their care. To A. D. ABEGG and D. DERVANOSKI for their assistance in analyzing collection material and obtaining natural history data of specimens. We thank L. M. CÔRREA (IBSP) for kindly assisting with laboratory protocols for DNA extraction and the PCR methodology. OME-N thanks Fundação de Amparo à Pesquisa do Estado de São Paulo (FAPESP, 2021/13671-7) and Coordenação de Aperfeiçoamento de Pessoal de Nível Superior (CAPES, 88887.667258/2022-00, 88887.986707/2024oo). TBG thanks Fundação de Amparo à Pesquisa do Estado de São Paulo (FAPESP, 2022/09428-2). This work was supported by Fundação de Amparo à Pesquisa do Estado de São Paulo (FAPESP 2016/50127-5; 2022/12660-4) and it is also part of the project "Evolution and biogeography of the herpetofauna: patterns, process and implications for conservation in scenario of environmental and climate changes" also funded by FAPESP (2021/07161-6).

References

- ALVARES, D. J., A. FERRARI & M. BORGES-MARTINS (2022): Geographic distribution patterns of amphibians and reptiles from the Uruguayan Savanna. Systematics and Biodiversity, 20: 1–17.
- ANDJELKOVIC, M., L. TOMOVIC & A. IVANOVIC (2016): Variation in skull size and shape of two snake species (*Natrix natrix* and *Natrix tessellata*). Zoomorphology, **135**: 243–253.
- Arnold, S. J. (1993): Foraging theory and prey size-predator size relations in snakes. pp 87–115 in: Seigel, R. A. & J. T. Collins (eds): Snakes: ecology and behavior. McGraw-Hill, New York.
- BARBO, F. E., W. W. BOOKER, M. R. DUARTE, B. CHALUPPE, J. A. PORTES-JUNIOR, F. FRANCO & F. G. GRAZZIOTIN (2022): Speciation process on Brazilian continental islands, with the description of a new insular lancehead of the genus *Bothrops* (Serpentes, Viperidae). Systematics and Biodiversity, 20: 1–25.
- BACHMAN, S., J. MOAT, A. W. HILL, J. DE LA TORRE & B. SCOTT (2011): Supporting Red List threat assessments with GeoCAT: geospatial conservation assessment tool. Zookeys, **150**: 117–126.
- BULLOCK, R. E. & W. W. TANNER (1966): A comparative osteological study of two species of Colubridae (*Pituophis* and *Thamnophis*). Brigham Young University Science Bulletin Biological Series, **8**: 1–29.
- CABRERA, A. L. & A. WILLINK (1973): Biogeografía de América Latina. – Programa Regional de Desarrollo Científico y Tecnológico, Washington DC.

- Costa, H. C. & R. S. Bérnils (2018): Répteis do Brasil e suas unidades federativas: lista de espécies. Herpetologia Brasileira, 1: 11–48.
- Cundall, D. & F. Irish (2008): The snake skull. pp. 349–692 in: Gans, C., A. S. Gaunt & K. Adler (eds): Biology of Reptilia. The Skull of Lepidosauria. Society for the Study of Amphibian and Reptiles Press, USA.
- Curcio, F. F., P. M. S. Nunes, M. B. Harvey & M. T. Rodrigues (2011): Redescription of *Apostolepis longicaudata* (Serpentes: Xenodontinae) with comments on its hemipenial morphology and natural history. Herpetologica, **67**: 318–331.
- Dowling, H. G. (1951): A proposed standard system of counting ventrals in snakes. British Journal of Herpetology, 1: 97–99.
- Drummond, A., B. Ashton, S. Buxton, M. Cheung, A. Cooper, C. Duran & A. Wilson (2010): Geneious Pro. Geneious. Biomatters Ltd, Auckland.
- EDGAR, R. C. (2004): MUSCLE: multiple sequence alignment with high accuracy and high throughput. – Nucleic Acids Research, 32: 1792–1797.
- Entiauspe-Neto, O. M., A. de Sena, A. Tiutenko & D. Loebmann (2019): Taxonomic status of *Apostolepis barrioi* Lema, 1978, with comments on the taxonomic instability of *Apostolepis* Cope, 1862 (Serpentes, Dipsadidae). Zookeys, **841**: 71–78.
- Entiauspe-Neto, O. M., C. Koch, T. B. Guedes & A. Tiutenko (2020a): Revisiting the taxonomic status of *Apostolepis sanctaeritae*, a forgotten Neotropical dipsadid snake. Salamandra, **56**: 329–341.
- Entiauspe-Neto, O. M., T. B. Guedes, D. Loebmann & T. Lema (2020b): Taxonomic status of two simultaneously described *Apostolepis* Cope, 1862 species (Dipsadidae: Elapomorphini) from Caatinga enclaves moist forests, Brazil. Journal of Herpetology, **54**: 225–234.
- ENTIAUSPE-NETO, O. M., G. M. F. RANGEL, T. B. GUEDES & A. TIUTENKO (2020c): Raising of Lazarus: Rediscovery and redescription of *Apostolepis niceforoi* Amaral, 1935 (Serpentes: Dipsadidae: Elapomorphini). Holotipus, 1: 21–35.
- Entiauspe-Neto, O. M., C. Koch, R. J. Gray, A. Tiutenko, D. Loebmann & T. B. Guedes (2021a): On the identity of *Apostolepis tertulianobeui* Lema, 2004 and integrative revision of *Apostolepis assimilis* (Reinhardt, 1861) (Serpentes: Dipsadidae). Zoologischer Anzeiger, 291: 123–138.
- Entiauspe-Neto, O. M., C. Koch, M. B. Harvey, G. R. Colli & T. B. Guedes (2021b): Redescription of *Apostolepis ambiniger* (Peters, 1869) (Serpentes: Dipsadidae: Elapomorphini). Vertebrate Zoology, 71: 231–251.
- Entiauspe-Neto, O. M., A. D. Abegg, C. Koch, L. P. Nuñez, W. D. S. Azevedo, L. J. Moraes, A. Tiutenko, T. S. Bialves & D. Loebmann (2021c): A new species of *Erythrolamprus* (Serpentes: Dipsadidae: Xenodontini) from the savannas of northern South America. Salamandra, 57: 196–218.
- Entiauspe-Neto, O. M., C. Koch, T. B. Guedes, R. C. B. Paradero, A. Tiutenko & D. Loebmann (2022): Unveiling an enigma from the Cerrado: taxonomic revision of two sympatric species of *Apostolepis* Cope, 1862 (Dipsadidae: Xenodontinae: Elapomorphini) from central Brazil. European Journal of Taxonomy, 817: 143–182.
- Felsenstein, J. & H. Kishino (1993): Is there something wrong with the bootstrap on phylogenies? A reply to Hillis and Bull. Systematic Biology, 42: 193–200.

- Ferrarezzi, H. (1993): Sistemática filogenética de *Elapomorphus*, *Phalotris* e *Apostolepis* (Serpentes, Colubridae, Xenodontinae). PhD dissertation, Universidade de São Paulo, Brazil
- Ferrarezzi, H. (1994): Uma sinopse dos gêneros e classificação das serpentes (Squamata): II. Família Colubridae. pp. 81–91 in: Nascimento, L. B., A. T. Bernardes & G. A. Cotta (eds): Herpetologia no Brasil 1. PUCMG, Belo Horizonte.
- Ferrarezzi, H., F. E. Barbo & C. E. Albuquerque (2005): Phylogenetic relationships of a new species of *Apostolepis* from Brazilian cerrado, with notes on the *assimilis* group (Serpentes: Colubridae: Xenodontinae: Elapomorphini). Papéis Avulsos de Zoologia, 45: 215–229.
- Felsenstein, J. (1985): Phylogenies and the comparative method.

 American Naturalist, 125: 1–15.
- GIRAUDO, A. R. & G. J. SCROCCHI (1998): A new species of *Apostolepis* (Serpentes: Colubridae) and comments on the genus in Argentina. Herpetologica, **54**: 470–476.
- GOLOBOFF, P. A., J. S. FARRIS & K. C. NIXON (2008): TNT, a free program for phylogenetic analysis. Cladistics, 24: 774–786.
- Guedes, T. B., C. Nogueira & O. A. V. Marques (2014): Diversity, natural history, and geographic distribution of snakes in the Caatinga, Northeastern Brazil. Zootaxa, 3863: 1–93.
- HARVEY, M. B. (1999): Revision of Bolivian *Apostolepis* (Squamata: Colubridae). Copeia, **1999**: 388–409.
- Instituto Chico Mendes de Conservação da Biodiversidade (2018): Livro vermelho da fauna Brasileira ameaçada de extinção: Volume IV Répteis. in: Instituto Chico Mendes de Conservação da Biodiversidade (Org.): Livro vermelho da fauna Brasileira ameaçada de extinção. ICMBio, Brasília.
- JOLIFFE, L. T. & J. CADIMA (2016). Principal component analysis: a review and recent developments. Philosophical Transactions of the Royal Society A: Mathematical, Physical and Engineering Sciences, 374(2065), 20150202.
- KATOH, K. & D. M. STANDLEY (2013): MAFFT multiple sequence alignment software version 7: improvements in performance and usability. Molecular Biology and Evolution, 30: 772–780
- Kearse, M., R. Moir, A. Wilson, S. Stones-Havas, M. Cheung, S. Sturrock & A. Drummond (2012): Geneious Basic: an integrated and extendable desktop software platform for the organization and analysis of sequence data. Bioinformatics, 28: 1647–1649.
- Kocher, T. D., W. K. Thomas, A. Meyer, S. V. Edwards, S. Pää-Bo, F. X. Villablanca & A. Wilson (1989): Dynamics of mitochondrial DNA evolution in animals: amplification and sequencing with conserved primers. – Proceedings of the National Academy of Sciences of the USA, **86**: 6196–6200.
- KNIGHT, A. & D. P. MINDELL (1994): The phylogenetic relationship of Colubrinae, Elapidae and Viperidae and the evolution of front-fanged venom systems in snakes. Copeia, 1994: 1–9.
- LAWSON, R., J. B. SLOWINSKI, B. I. CROTHER & F. BURBRINK (2005): Phylogeny of the Colubroidea (Serpentes): New evidence from mitochondrial and nuclear genes. Molecular Phylogenetics and Evolution, 37: 581–601.
- Lanfear, R., P. B. Frandsen, A. M. Wright, T. Senfeld & B. Calcott (2017): PartitionFinder 2: new methods for selecting partitioned models of evolution for molecular and morphological phylogenetic analyses. Molecular Biology and Evolution, 34: 772–773.

- LEMA, T. D. (1993): Polimorfismo em *Apostolepis dimidiata* (Jan, 1862) com a invalidação de *Apostolepis villaricae* Lema, 1978 e *Apostolepis barrioi* Lema, 1978 (Serpentes: Colubridae: Xenodontinae: Elapomorphini). Acta Biologica Leopoldensia, 15: 35–52.
- Lema, T. D. (2001): Fossorial snake genus *Apostolepis* from South America (Serpentes: Colubridae: Elapomorphinae). Cuadernos de Herpetología, **15**: 29–43.
- LEMA, T. D. & L. H. CAPPELLARI (2001): *Apostolepis quirogai*. Brazil: Rio Grande do Sul. Herpetological Review, **32**: 121.
- LEMA, T. D. (2002): Nova espécie de *Apostolepis* Cope do grupo dimidiata do Cerrado do Brasil (Serpentes: Elapomorphinae).
 Comunicações do Museu de Ciências e Tecnologia da PU-CRS Série Zoologia, 15: 227-238.
- Lema, T. D. (2003): Descrição de nova espécie de *Apostolepis* Cope do cerrado do Brasil, pertencente ao grupo *dimidiata* (Serpentes, Elapomorphinae). Acta Biologica Leopoldensia, **25**: 123–131.
- Lema, T. D. (2004): Nova espécie de *Apostolepis* Cope do estado de Rondônia, Brasil (Serpentes, Elapomorphinae). Comunicações do Museu de Ciências e Tecnologia da PUCRS, Série Zoologia, 17: 81–89.
- LEMA, T. D., F. M. D'AGOSTINI & L. H. CAPPELLARI (2005). Nova espécie de *Phalotris*, redescrição de *P. tricolor* e osteologia craniana (Serpentes, Elapomorphinae). Iheringia, Série Zoologia, **95**: 65–78.
- Lema, T. D. & C. H. Hofstadler-Deiques (2010): Description of a new genus for allocation of *Elapomorpus lepidus* and the status of *Elapomorphus wuchereri* (Serpentes: Dipsadidae: Xenodontinae: Elapomorphini). Neotropical Biology & Conservation, 5: 113–119.
- Lema, T. D. & M. F. Renner (2011): A new species of *Apostolepis* (Serpentes, Colubridae, Elapomorphini), belonging to *assimilis* group, found in Brazilian Cerrado. Ciência em Movimento, 13: 71–76.
- MACHADO, D. J. (2015): YBYRÁ facilitates comparison of large phylogenetic trees. BMC Bioinformatics, 16: 1–4.
- MacLachlan, G. J. (2004). Discriminant Analysis and Statistical Pattern Recognition. Wiley-Interscience, Hoboken.
- MORRONE, J. J. (2014): Biogeographical regionalisation of the Neotropical region. Zootaxa, 3782: 1–110.
- Montingelli, G. G., F. E. Barbo, G. A. Pereira Filho, G. G. Santana, F. G. R. França, F. G. Grazziotin & H. Zaher (2020): A second new species for the rare dipsadid genus *Caaeteboia* Zaher et al., 2009 (Serpentes: Dipsadidae) from the Atlantic Forest of northeastern Brazil. Cuadernos de Herpetología, 34: 219–230.
- NOGUEIRA, C. C., F. E. BARBO & H. FERRAREZZI (2012): Redescription of *Apostolepis albicollaris* Lema, 2002, with a key for the species groups of the genus *Apostolepis* (Serpentes: Dipsadidae: Elapomorphini). South American Journal of Herpetology, 7: 213–225.
- Noonan, B. P. & P. T. Chippindale (2006): Dispersal and vicariance: The complex evolutionary history of boid snakes. Molecular Phylogenetics and Evolution, **40**: 347–358.
- OLIVEIRA, L. D., F. G. GRAZZIOTIN, P. M. SÁNCHEZ-MARTÍN-EZ, M. SASA, O. FLORES-VILLELA, A. PRUDENTE & H. ZAHER (2023): Phylogenetic and morphological evidence reveals the association between diet and the evolution of the venom de-

- livery system in Neotropical goo-eating snakes. Systematics and Biodiversity, 21: 2153944.
- Olson, D. M., E. Dinerstein, E. D. Wikramanayake, N. D. Burgess, G. V. Powell, E. C. Underwood & K. R. Kassem (2001): Terrestrial ecoregions of the world: a new map of life on earth. A new global map of terrestrial ecoregions provides an innovative tool for conserving biodiversity. BioScience, 51: 933–938.
- Palumbi, S. R., A. Martin, S. Romano, W. O. McMillan, L. Stice & G. Grabowski (1991): The simple fool's guide to P.C.R. University of Hawaii Press, Honolulu.
- Paradis, E. & K. Schliep (2019): ape 5.0: an environment for modern phylogenetics and evolutionary analyses in R. Bio-informatics, 35: 526–528.
- POOK, C. E., W. WÜSTER & R. S. THORPE (2000): Historical biogeography of the western rattlesnake (Serpentes: Viperidae: *Crotalus viridis*), inferred from mitochondrial DNA sequence information. Molecular Phylogenetics and Evolution, 15: 269–282.
- Peters, J. A. (1964): Supplemental notes on snakes of the subfamily Dipsadinae (Reptilia: Colubridae). Studies on Neotropical Fauna and Environment, 4: 45–50.
- Qgis Development Team (2021): QGIS Geographic Information System. Version 3.16.3. Available from http://www.qgis.org, accessed 1 Aug. 2021.
- R Development Core Team (2015): R: a language and environment for statistical computing, Release 3.2. Available from http://cran.r-project.org, accessed 1 Aug. 2021.
- Revell, L. (2012): phytools: An R package for phylogenetic comparative biology (and other things). Methods in Ecology and Evolution, 3: 217–223.
- Rodrigues, M. T. (1993): Herpetofauna das dunas interiores do Rio São Francisco: Bahia: Brasil. V. Duas novas espécies de *Apostolepis* (Ophidia, Colubridae). – Memórias do Instituto Butantan, **54**: 53–59.
- Ruiz-Perez, D., H. Guan, P. Madhivanan, K. Mathee & G. Narasimham (2020): So you think you can PLS-DA? BMC Bioinformatics, 21: 1–10.
- SALVE (2023): Sistema de avaliação do risco de extinção da biodiversidade – Available from https://salve.icmbio.gov.br/, accessed 1 Aug. 2023.
- Sabaj, M. H. (2019): Standard symbolic codes for institutional resource collections in herpetology and ichthyology: an online reference. Version 6.5. American Society of Ichthyologists and Herpetologists, USA, available from http://www.asih.org, accessed 10 Sept. 2021.
- SAVITZKY, A. H. (1979): The origin of the New World proteroglyphous snakes and its bearing on the study of venom delivery systems in snakes. PhD dissertation, University of Kansas, USA.
- STAMATAKIS, A. (2014): RAXML version 8: a tool for phylogenetic analysis and post-analysis of large phylogenies. Bioinformatics, 30: 1312–1313.
- Soriano, A., R. J. C. León, O. E. Sala, R. S. Lavado, V. A. Dere-Gibus, M. A. Cahuepé, O. A. Scaglia, C. A. Velazquez & J. H. Lemcoff (1992): Río de la Plata grasslands. – pp. 367–407 in: Coupland, R. T. (ed.): Ecosystems of the World 8A. Natural Grasslands. – Elsevier, New York.
- Vaidya, G., D. J. Lohman & R. Meier (2011): SequenceMatrix: concatenation software for the fast assembly of multi-gene

- datasets with character set and codon information. Cladistics, **27**: 171–180.
- Yang, Z., S. Kumar & M. Nei (1995): A new method of inference of ancestral nucleotide and amino acid sequences. Genetics, 141: 1641–1650.
- Zaher, H. (1994): Phylogenie des Pseudoboini et evolution des Xenodontinae sud-americains (Serpentes, Colubridae). – PhD dissertation, Musée National D'Histoire Naturelle, France.
- Zaher, H. (1999): Hemipenial morphology of the South American xenodontine snakes, with a proposal for a monophyletic Xenodontinae and a reappraisal of colubroid hemipenes.

 Bulletin of the American Museum of Natural History, 240: 1–168.
- Zaher, H., F. G. Grazziotin, J. E. Cadle, R. W. Murphy, J. C. Moura-Leite & S. L. Bonatto (2009): Molecular phylogeny of advanced snakes (Serpentes, Caenophidia) with an emphasis on South American xenodontines: A revised classification and descriptions of new taxa. Papéis Avulsos de Zoologia, São Paulo, 49: 115–153.
- Zaher, H., M. Yánez-Muñoz, M. T. Rodrigues, R. Graboski, F. A. Machado, M. Altamirano-Benavides & F. G. Grazziotin (2018): Origin and hidden diversity within the poorly known Galápagos snake radiation (Serpentes: Dipsadidae). Systematics and Biodiversity, 16: 614–642.
- Zaher, H., R. W. Murphy, J. C. Arredondo, R. Graboski, P. Machado-Filho, K. Mahlow & F. G. Grazziotin (2019): Large-scale molecular phylogeny, morphology, divergence-time estimation, and the fossil record of advanced caenophidian snakes (Squamata: Serpentes). PLoS ONE, 14: e0216148.
- Zar, J. H. (1999): Biostatistical Analysis. 4^{th} edition. Prentice Hill, Upper Saddle Hill.

Supplementary data

The following data are available online:

Supplementary Material 1. Material examined.

Supplementary Material 2. Parsimony based morphological character analysis and NEXUS input file.

Supplementary Material 3. Taxon and character matrix used in morphological analysis, in Phylip format.

Supplementary Material 4. Putative morphological synapomorphies identified by YBYRÁ software.

Supplementary Table 1. Primers used in this study to amplify gene fragments.

Supplementary Table 2. Best-fit partitions and models for PartitionFinder 2 concatenated analysis.

Supplementary Figure 1. Boxplots, scatterplots, histograms, density plots, and pairwise comparison of selected characters of external morphology in males and females of *Apostolepis quirogai*.

Supplementary Figure 2. Molecular distance analyses for *Apostolepis* terminals.

Supplementary Figure 3. Micro-CT images of the skull without mandibles of *Apostolepis quirogai* in dorsal view.

Supplementary Figure 4. Micro-CT images of the skull without mandibles of *Apostolepis quirogai* in ventral view.

Supplementary File 1. Dataset 1, evaluated morphological character in *Apostolepis* species used in Principal Component Analyses (PCA), Partial Least Squares Discriminant Analyses (PLS-

DA), Discriminant Function Analyses (DFA), and Jackknife cross-validation test.

Entiauspe-Neto et al-1699-Supplementary File 1.csv

Supplementary File 2. Taxon and gene sampling used in molecular phylogenetic analyses, modified from Zaher et al. (2018). Taxa in bold were generated in this study and will be deposited in GenBank upon acceptance of manuscript.

Entiauspe-Neto_et_al-1699-Supplementary_File_2.xlsx

Supplementary File 3. Phylogenetic relationships of Caenophidia, under Maximum Likelihood (RAxML) hypothesis.

 $Entiauspe-Neto_et_al-1699-Supplementary_File_1.pdf$

Supplementary File 4. Overview of PCA and DFA autovectors, analyses output, and Jackknife classificatory matrixes. Entiauspe-Neto_et_al-1699-Supplementary_File_4.rar